# Structures of Hippuristanol and Pateamine A Analog MZ735 in Complex with EIF4A

Jason Liang

Department of Biochemistry

McGill university

Montreal, QC

July 2020

A thesis submitted to McGill University in partial fulfillment of the requirements of the degree of master's in Biochemistry

© Jason Liang, July 2020

# Acknowledgements

I firstly and foremost would like to thank my family for providing me with support and encouragement throughout my research and studies. Secondly, I would like to thank my supervisor, Dr. Bhushan Nagar, for providing me the opportunity for research and the guidance in completing it. Thirdly, I would like to thank the other members of my laboratory for the help they have provided me. Dr. Alexei Gorelik has provided much aid in both learning crystallography and mentoring, for which I would give him my deepest thanks. I would like to thank Dr. Heidi Olesen, who initially taught me the basics and for her patience. Dr. Katalin Iles has been extremely helpful in preparing cultures and Dr. Jonathan Labriola has also been extremely helpful when I needed further clarifications and running mass spectrometry. In terms of collaborators, I would like to thank Dr. Pelletier for proposing the initial project and providing valuable information and data throughout the project. I would like to thank Sai Kai Nareem from the Pelletier lab who has been a great help in preparing solutions and providing enzymatic data. I would like to thank the chemists, Dr. Kenneth Hull, and Dr. Daniel Romo from Baylor University, who have collaborated by providing ligands for the structures.

# Preface

This thesis is the bases of a manuscript to which I contribute as an author. The contribution of the co-authors is as follows,

Naineni S. K.*, Liang, J.*, Zhu, M., Hull, K. G., Romo, D., Nagar, B.*, Pelletier, J.*

* Equal contribution

Author contributions:

Constructs were provided by the Pelletier lab (Sai and Jerry Pelletier). Purifications, crystallizations, and assays, unless otherwise mentioned, were performed by me. Solving the structure and data collection was also done by me. Dr. Bhushan Nagar supervised my portion of the work.

# Table of Contents

# List of Figures

# Abstract

eIF4A is a component of the eIF4F complex and an important regulating factor for protein translation. Its function is necessary for the efficient translation of transcripts that are under secondary structure control. eIF4A functions as an RNA helicase, allowing “melting” of mRNA secondary structure present in the template. These roadblocks would normally impede the movement of the ribosome, thus blocking translation of the mRNA. Sequences under this type of control are often involved in tightly regulated processes, such as cell growth and replication. As such, mutations in proteins may lead to cancers when freed from their normal regulatory elements. Therefore, eIF4A is a potential target for anti-cancer drugs. In terms of inhibitors, recently a structure with rocaglamide (a potent eIF4A inhibitor) and RNA was published, allowing a complete understanding of how the ligand interacts with the protein. In this thesis, other potential inhibitors with different chemical scaffolds were structurally explored, specifically hippuristanol and a pateamine A, analog MZ735. Crystallization of eIF4A with RNA and MZ735 was successful. Surprisingly, although the structures of MZ735 and rocaglamide differ quite considerably, MZ735 binds to eIF4A in the same manner as rocaglamide. These results provided a basis for pateamine A-like compounds binding and will guide development of new inhibitors.

# Résumé

eIF4A (facteur d’initiation eucaryote 4A) est un composant du complexe eIF4F et un facteur régulateur pour la traduction des protéines. Sa fonction est nécessaire pour la traduction efficace des transcriptions sous contrôle de structure secondaire. eIF4A fonctionne en tant qu’hélicase d'ARN, permettant la dissolution de la structure secondaire ARN messager présente dans la matrice. Ces structures entraveraient normalement le mouvement du ribosome, bloquant ainsi la traduction de l'ARNm. Les séquences sous ce type de contrôle sont souvent impliquées dans des processus étroitement régulés, tels que la croissance et la réplication cellulaires. Les mutations de ces protéines peuvent causer des cancers lorsqu'elles sont libérées de leurs éléments régulateurs. Par conséquent, eIF4A est une cible potentielle pour les médicaments anticancéreux. Une structure de eIF4A avec rocaglamide (un puissant inhibiteur) et l’ARN a récemment été publiée, permettant une compréhension complète de la façon dont le ligand interagit avec la protéine. Dans cette thèse, d'autres inhibiteurs potentiels avec différentes caractéristiques chimiques ont été explorés structurellement, en particulier l'hippuristanol et un analogue de pateamine A, MZ735. La cristallisation de eIF4A avec l'ARN et MZ735 a réussi. Étonnamment, bien que les structures du MZ735 et du rocaglamide diffèrent considérablement, MZ735 se lie à eIF4A de la même manière que le rocaglamide. Ces résultats ont fourni une base pour la liaison des composés de type pateamine A et guideront le développement de nouveaux inhibiteurs.

# 1 Literature review

## 1.1 Introduction

Translation is a process involving a wide variety of proteins. Although the key component is the ribosome, which ultimately assembles the polypeptide chain, other proteins are necessary for the process to initiate and progress without interruption. For example, the eRFs (eukaryotic release factor) allow proper termination of translation upon the recognition of a termination codon. Translation initiation is another regulated process, which requires assistance from different proteins. These proteins ensure that the mRNA is properly processed before the ribosome is recruited for efficient translation. This thesis will focus on the eIF4F (eukaryotic initiation factor 4F) complex, the first complex which interacts with mRNA and begins the process of mRNA translation initiation. eIF4A (a component of the complex) will be the focus of this review, with an emphasis on its function, regulation, and structure.

## 1.2 eIF4F function

The eIF4F complex is an important protein assembly involved in translation [1]. This complex allows the processing of mRNA, preparing it for efficient translation by allowing the recruitment of the ribosome and the processing of mRNA [2]. The complex is composed of three proteins (eIF4A, eIF4E and eIF4G) and is associated with two others: eIF4B and eIF4H [1, 3, 4]. eIF4A is a helicase enzyme, which removes mRNA secondary structure such as stem-loops and G-quadruplexes that would normally prevent mRNA translation, due to the ribosome's inability to bypass such obstacles [5]. This process, as with other helicases, is ATP-dependent [2]. eIF4E recognizes the 5' $m^7$GTP cap of processed mRNA, ensuring translation of only mature RNA [6]. eIF4G is involved in scaffolding for the complex, interacting with both eIF4A and eIF4E [7]. It also associates with PABP (poly A binding protein) which allows the circularization of mRNA

by connecting the poly-A tail to the cap (which is bound by eIF4E). It is also involved in translation initiation at internal ribosome entry sites (IRES), referred to as cap-independent translation [8]. A visual reference on how these factors interact in translation initiation is displayed in Figure 1.

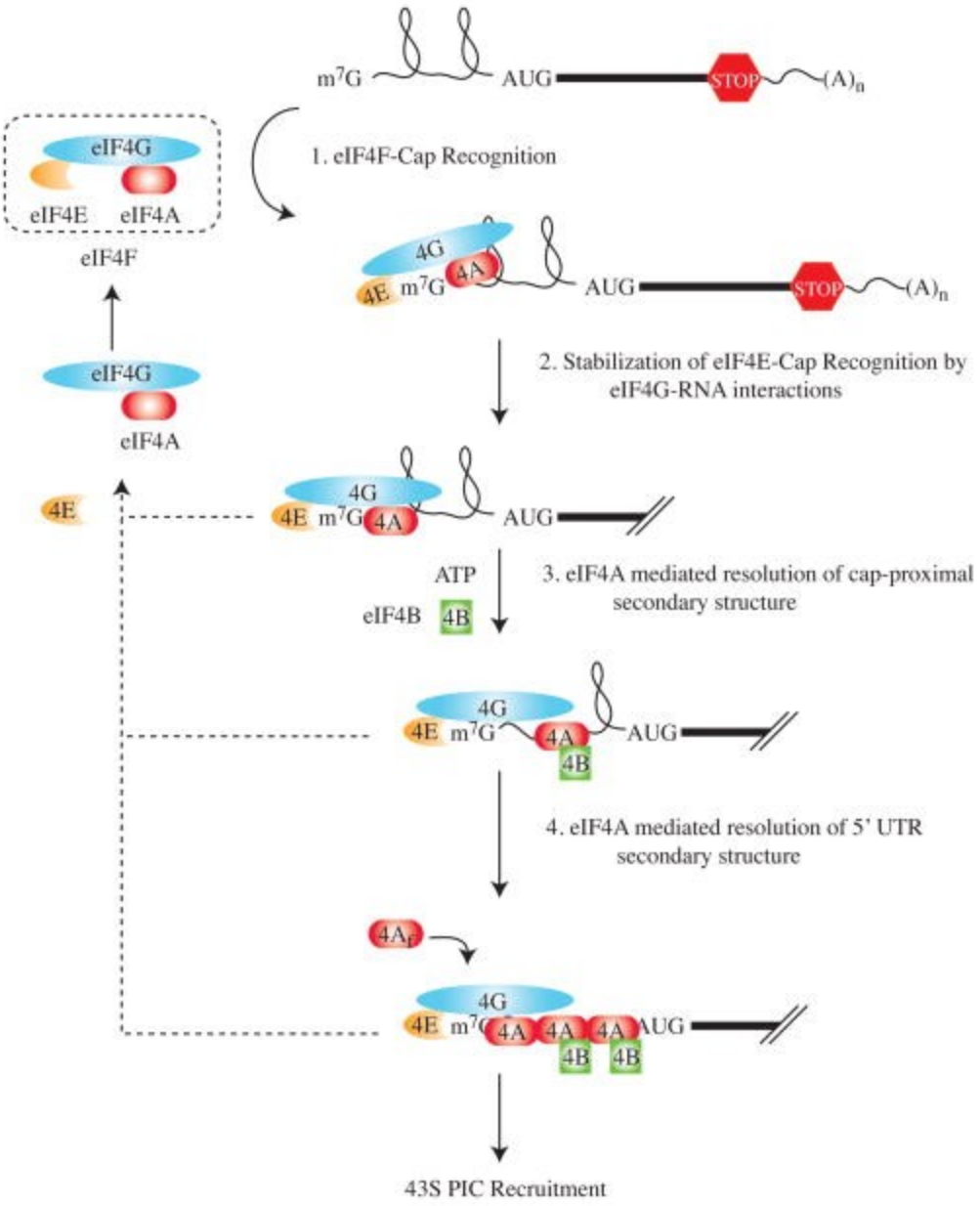


**Figure 1** – A diagram of eIF4F function on mRNA. eIF4F recognizes the mRNA $m^7GTP$ cap through eIF4E, which then allows multiple rounds of eIF4A unwinding of any 5' UTR secondary structure. Once secondary structure has been removed, the 43S preinitiation complex may be recruited to scan the mRNA for the initiation codon. eIF4G-PABP interaction has been taken out for clarity. Figure 1 taken from Pelletier, et al. [9]

eIF4B and eIF4H are RNA-binding proteins, that function as enhancing factors [10, 11]. They associate with eIF4A mutually exclusively on the same binding site [11]. Both proteins modulate eIF4A affinity for ATP and RNA [11]. Another function of 4B and 4H is to stabilize regions of

unwound RNA and prevent reannealing of the RNA after processing [10]. eIF4B is required for 48S initiation complex formation on any sequence with a moderate amount of 5' UTR complexity [12]. eIF4H allows eIF4A to bind more readily to loop structures formed on the strand of mRNA [13]. eIF4AII is a paralog of eIF4A, present in mammals [14]. It undergoes differential expression dependent on cellular growth status in mice [15]. Although its purpose is still unclear, it does not appear to be necessary for cell viability or protein synthesis [14]. eIF4AIII is also a member of the eIF4A family, however it has a more specific role: it preferentially associates with spliced mRNA and binds mRNA at the position of the exon junction complex (the protein complex which forms near exon-exon junctions of mRNA due to splicing) [16].

## 1.3 eIF4F control and disease

Given the critical role of the eIF4F complex in translation initiation, it is not surprising that its components are tightly regulated. eIF4E has been extensively studied, through its involvement in the mTOR signalling pathway [17]. This pathway is implicated in the cell survival, regulated by nutrients, growth factors and energy metabolism (ATP) [17]. eIF4E is the limiting factor in the eIF4F complex, being present in the lowest concentrations of all subunits [18]. eIF4E is controlled by 4E-BP (4E-binding protein) which, when bound to eIF4E, prevents the association of the protein to the eIF4F complex [19]. This impairs the ability of the complex to associate to mRNA, reducing cap-dependant translational initiation [19]. mTOR is the kinase controlling the activity of 4E-BP; when 4E-BP is phosphorylated, it cannot interact with eIF4E, releasing eIF4E from its inhibition [20]. mTOR is part of two multiprotein complexes, mTORC1 and mTORC2, which regulate proteins controlling cell growth and proliferation [20]. mTORC1 is the complex

which interacts with 4E-BP, and controls mitochondrial activity and adipogenesis, while mTORC2 regulates cytoskeletal dynamics and mitochondrial physiology [20].

eIF4B is controlled by the mTOR/PI3K pathway in conjunction with the ras/MAPK pathway [21]. These cascades control the phosphorylation of Ser406 on eIF4B, which is important for optimal translation [22]. Ser422 may be phosphorylated, which was demonstrated as necessary for translation through mutational assays [23]. The Ser422Glu mutation results in similar activity to wild type, whereas Ser422Ala mutant which cannot be phosphorylated is inert [23].

eIF4G can be phosphorylated by the kinase Pak2 [24]. This inhibits the association between eIF4G and eIF4E and may subsequently inhibit eIF4F function, by making it less likely to associate to the $m^7$GTP cap [24]. PAIPII may bind PABP, in competition with eIF4G [25]. By disrupting the PABP-eIF4G interaction, the cyclization of mRNA will be prevented, and results in less efficient translation [25].

eIF4A is under the control of PDCD4 (programmed cell death protein 4) [26]. PDCD4 is involved in apoptosis, normally under control by S6 kinase-mediated phosphorylation (which results in ubiquitination and degradation of the PDCD4) [27]. S6 kinase itself is under mTORC1 control [26]. PDCD4, when left undegraded, can sequester two molecules of eIF4A, preventing their recruitment into eIF4F [26]. Without eIF4A, the eIF4F complex is unable to process mRNA secondary structure, resulting in the inability of the ribosome to translate sequences under secondary structure control, due to roadblocks in scanning [26].

It is not surprising that deregulation of these proteins is linked to several cancers. eIF4E, 4B and 4A are all affected by pathways which are common in cancer development (PI3K and ras/MAPK) [28, 29]. PDCD4 is a tumor suppressor protein, where downregulation of PDCD4

increases mobility and invasiveness of tumor cells [30, 31]. Deregulation of the mTOR pathway is connected to numerous cancers and increased activation is often associated with resistance to cancer therapies [32]. mTOR inhibitors have also been shown to provide antitumor effects in lung cancer [33]. Drugs involving eIF4F inhibition have potential as anti-cancer tools, due to its key role in recruiting the ribosome [34]. Many genes which contain secondary structure in the 5' UTR, regulate critical cellular processes (cell growth, survival, proliferation and migration), which are deregulated in cancers [9]. Potential inhibitors of eIF4A have been found from natural products, for example hippuristanol (extracted from *Isis hippuris*), rocaglamide (discovered in *Aglaia elliptifolia*) and pateamine A (discovered in *Mycale hentscheli*), which all have shown promise in inhibiting cancer development in cell assays [35-37].

## 1.4 eIF4A

With how the eIF4F complex hinges on eIF4A's proper functioning and regulation, a deeper examination of eIF4A is necessary. eIF4A is the prototypical member of the DEAD-box family, a family of related ATPases (RNA-associated proteins involved with a variety of cellular processes, such as transcription, pre-mRNA processing, nuclear mRNA export, translation initiation among others) [38]. All the proteins in the family contain nine characteristic motifs, flanked by less conserved motifs (most likely due to the variety of substrates the family members interact with) [38]. These motifs share similarities with other RNA helicase families, but the conserved sequences are modified (DEAH-box family members have a histidine instead of aspartate for example) [38]. Motifs which interact with other molecules are displayed in Figure 2 [39].

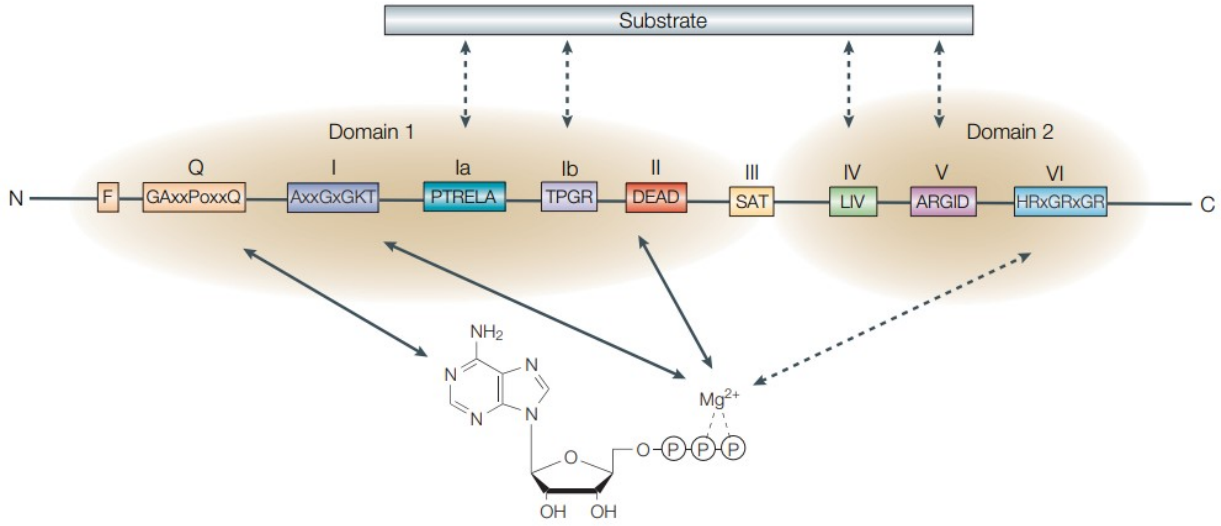


**Figure 2** – eIF4A interactions with other molecules. Conserved domains of eIF4A are present in the NTD and CTD. Q motif interacts with the adenosine from the ATP, and motif I, II and VI (to a lesser extent) interact with the magnesium ion coordinated with ATP. Ia, Ib, IV and V have been identified interacting with RNA. Figure 2 taken from Rocak, et al. [39].

eIF4A contains two RecA-like domains [referred to as NTD (N-terminal domain) and CTD (carboxy-terminal domain)] connected by a short linker [40]. The nucleotide cycle of DEAD-box proteins has been documented through FRET experiments [41]. Upon binding of RNA and ATP, eIF4A adopts a more closed conformation [41]. In the closed state, the protein may induce a kink in the mRNA strand, thus physically destabilizing any secondary structure [42]. The protein remains closed until ATP hydrolysis occurs [42]. Reopening of the protein occurs when phosphate is released, and RNA dissociates [43]. This cycle may then be resumed by exchanging the ADP for ATP [43]. The dependency on eIF4A for translation is directly correlated with secondary structure associated with a mRNA sequence, with oncogenes associated with more secondary structure [44]. These sequences are subsequently most impacted by eIF4A inhibition [45]. Inhibition of eIF4A may occur in various fashions, through interactions with other proteins (previously discussed) or through use of chemical inhibitors. These inhibitors may then inhibit targeting different areas of eIF4A activity. For example, preventing eIF4A from entering a

closed conformation or interfering with how RNA binds to eIF4A. Many natural products were identified through screening, inhibiting eIF4A by preventing RNA from interacting with the protein by blocking the site where RNA binds or increasing RNA affinity, such that eIF4A cannot effectively scan the mRNA [9]. Recently, other screens for eIF4A ATPase inhibitors have been explored [46]. Sanguinarine is an inhibitor which operates by occupying the same binding pocket as ATP and prevents the formation of the closed conformation of eIF4A [47]. Although there are numerous methods of inhibiting eIF4A, this review will focus on two compounds, hippuristanol and MZ735, that are being studied in Dr. Jerry Pelletier's lab at McGill University for their inhibitory action on eIF4A.

## 1.5 eIF4A inhibition

### 1.5.1 Hippuristanol

Hippuristanol belongs to one of four classes of polyoxygenated steroids [48]. All these classes have been tested for cytotoxic activity on cancer cell lines, with the hippurin/hippuristanol class having the highest potency [49]. A key distinction explaining the difference in activity is the presence of spiroketal rings (shown in Figure 3) which are absent from the other classes [48].

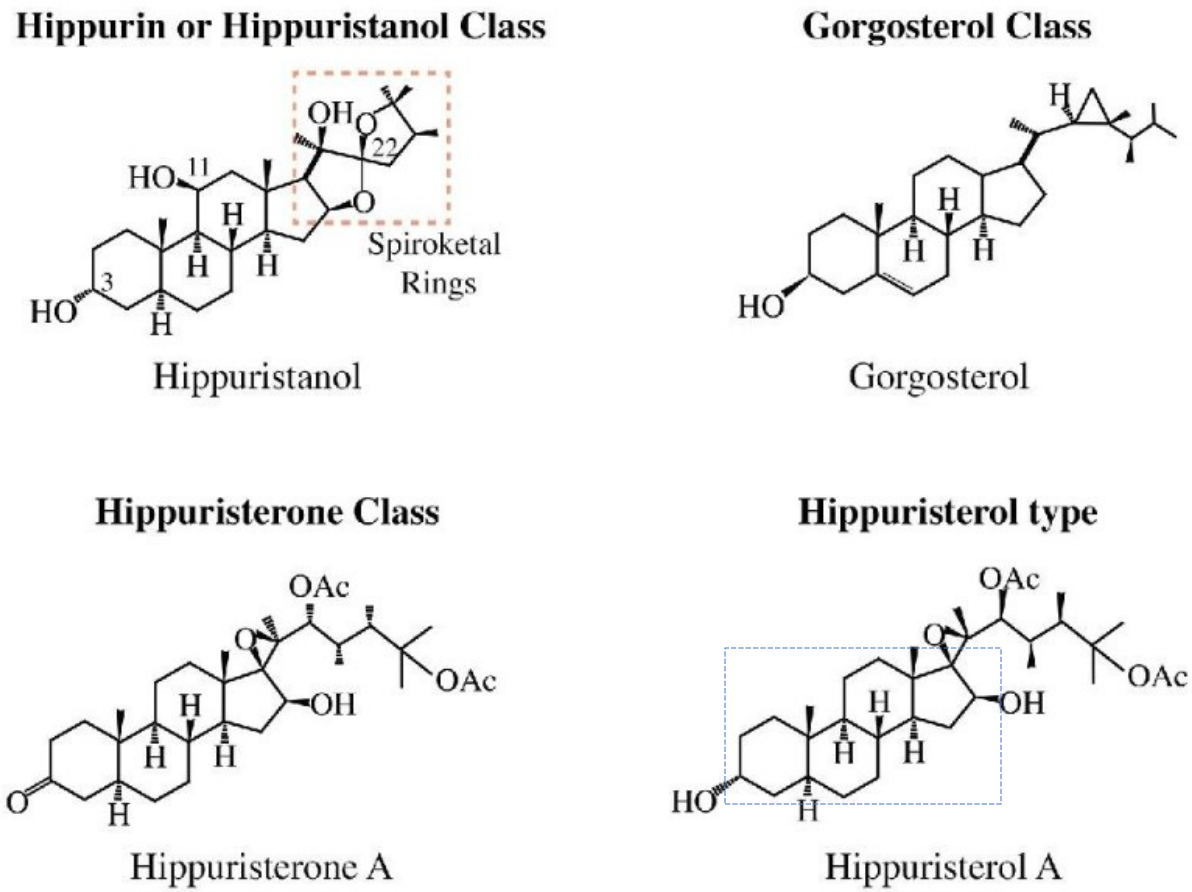


**Figure 3** – Polyoxygenated steroid classes. Structures of all classes of polyoxygenated steroids (cholesterol ring boxed in blue), outlining the major differences between hippurin/hippuristanol in comparison to the other classes. Figure 3 taken from Cencic, et al. [48]

Hippuristanol inhibits translation by preventing eIF4A from interacting with RNA [36]. This is accomplished in an ATP-independent manner and operates on both free eIF4A and as part of the eIF4F complex [36]. Nuclear magnetic resonance (NMR) experiments have identified residues involved in the binding of hippuristanol [50]. Residues in motifs V and VI appear to interact with hippuristanol [50]. Hippuristanol itself has also been examined; SAR (structure-activity relationships) have been identified, emphasizing key structural points necessary for activity, shown in Figure 4 [48].

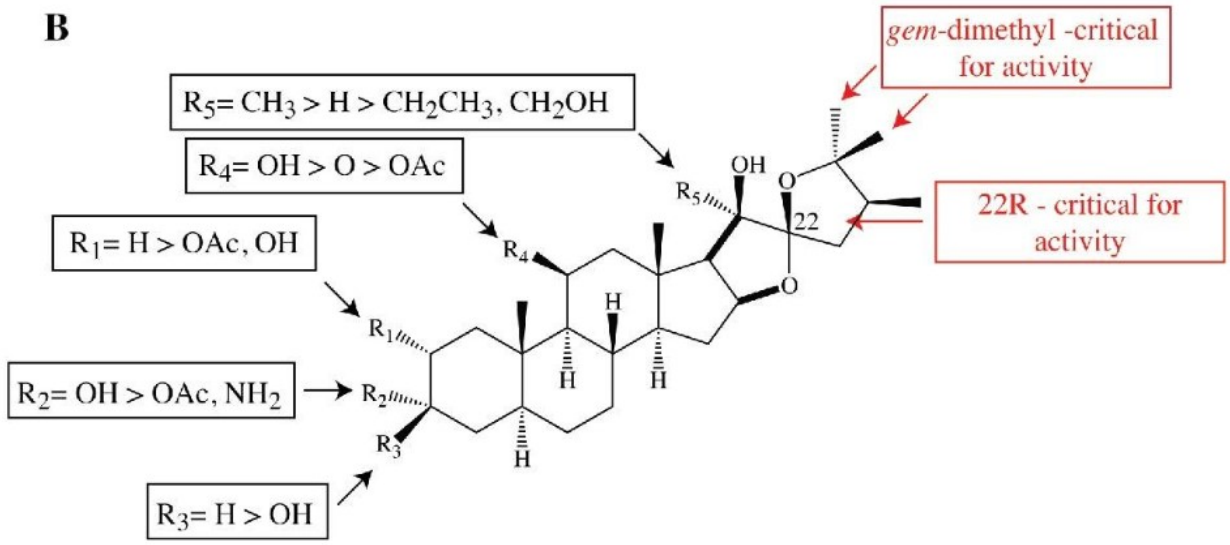


**Figure 4** – Hippuristanol Structure and Activity Relationships (SAR). Analogs were synthesized through parallel routes and had activity quantified through inhibition of HeLa cell proliferation. Other necessary structural components have been highlighted in red. Figure 4 taken from Cencic, et al. [48]

The gem-dimethyl substitution on the F ring and chirality of carbon 22 were determined to be critical for activity [51].

Hippuristanol has demonstrated anti-neoplastic activity in both vivo and vitro systems [52]. It inhibited the growth of DBA/MC fibrosarcoma cells and exhibited in vivo activity against lymphocytic leukemia P-388 tumors in mice [52]. It was also observed that hippuristanol inhibited adult T-cell leukemia in vitro and in vivo in a xenograft model [53]. When tested for cell viability against healthy peripheral blood mononuclear cells from patients with adult T-cell leukemia, hippuristanol was found to have a reduced effect, strengthening its potential use as a therapeutic agent [53]. When tested against JJN-3 multiple myeloma cell viability, $IC_{50}$ of hippuristanol was determined as around 0.100 μM – 0.300 μM [54, 55].

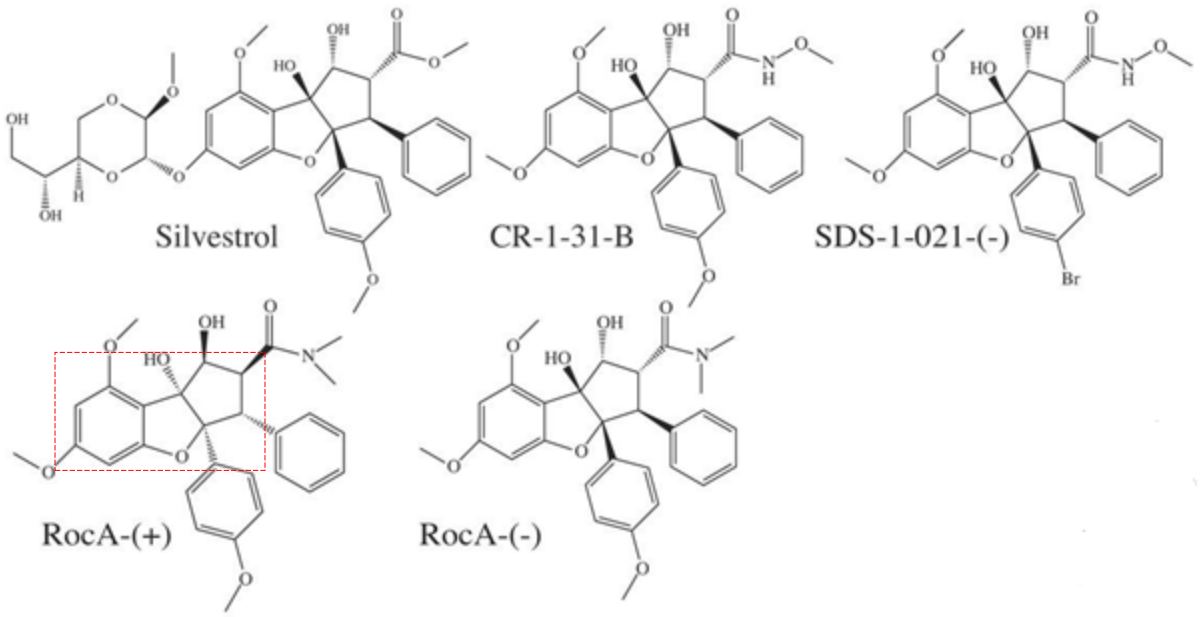


**Figure 5** – Structure of different rocaglates. Key structural feature of rocaglates is the cyclopenta[b]benzofuran skeleton (outlined in red). Figure 5 taken from Chu, et al. [56]

### 1.5.2 Rocaglates

Rocaglates inhibit eIF4A by stabilizing the interaction of poly-purine RNA and eIF4A. This results in eIF4A being unable to properly remove secondary RNA structure and remains associated to RNA [57]. This association is ATP-independent and creates a roadblock for incoming ribosomes, resulting in the ribosome falling off [57]. Key identifying factors of rocaglates is the cyclopenta[b]benzofuran core (as shown in Figure 5) [58]. Rocaglates such as rocaglamide and silvestrol have been identified, showing the most favorable pharmacological properties for in vivo studies [9]. Silvestrol has 100% systemic availability when delivered intraperitoneally and 60% remains after 6 hours, while causing no liver damage, weight loss or immunosuppression in mice [59, 60]. B-cells from chronic leukemia patients are more sensitive than B-cells from healthy individuals, suggesting preferential targeting of faster growing leukemic cells [61]. When tested against JJN-3 multiple myeloma cell viability, the $IC_{50}$ of silvestrol was determined as lower than 10 nM [55]. Rocaglamide has been identified as a top hit

in screens, effective in killing cells with aneuploidy and those driven by MYC activation [62]. When tested against HEK293 cell viability, rocaglamide had an $IC_{50}$ of 3.68 nM [62].

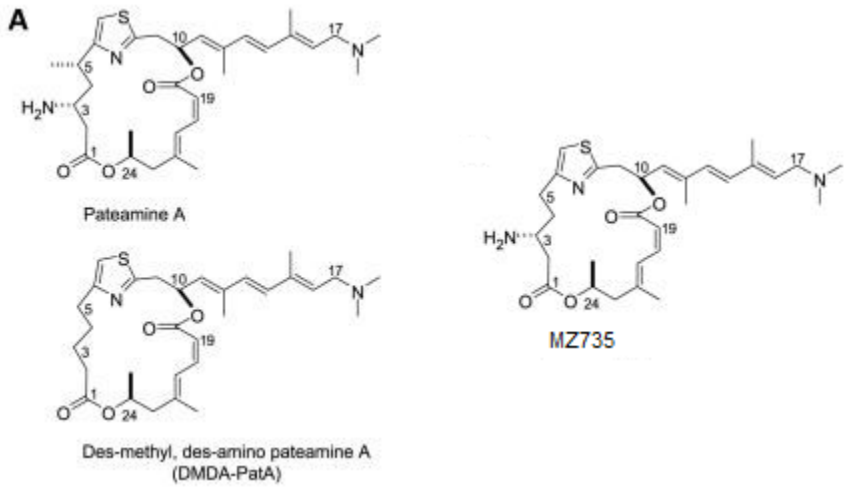


**Figure 6 –** Structure of pateamine A and synthesized analogs DMDA-PatA and MZ735. Differences between the molecules are the substitutions on the 3 and 5 carbons. Figure 6 adapted from Kuznetsov, et al. [63]

### 1.5.3 Pateamine A

Pateamine A (and associated analogs) is another compound discovered to inhibit eIF4F through eIF4A binding [35]. Their chemical structure includes a large twenty-membered ring with a thiazole ring, two esters and a triene arm with a tertiary amine at its end (shown in Figure 6). In terms of inhibiting eIF4A, it increases eIF4A affinity for RNA, with the ability to inhibit cancer cell line proliferation in an irreversible fashion (HeLa and MCF-7 cells) [64]. An important differentiating factor between pateamine A and rocaglamide is that rocaglamide necessitates poly-purine RNA for proper function, whereas pateamine A and its analogs have no specificity for particular bases (Dr. Jerry Pelletier, unpublished data). Tests have shown in vitro and in vivo anticancer activity of both pateamine A and DMDA-PatA [63]. Derivatives for both pateamine A and DMDA-patA have undergone parallel synthesis resulting in the creation of multiple

compounds, which then had their activities quantified through in vitro assays [65]. MZ735 is one analogue, notable due to its large increased potency in inhibiting translation compared to other synthesized analogues (e.g. DMDA-patA) [66]. MZ735 displayed an $IC_{50}$ of 2.3 nM compared to DMDA-patA, which had an $IC_{50}$ of 21 nM in inhibiting c-Myc (a master transcription factor and oncogene) expression in lymphoma cell lines [66]. Both compounds had no cytotoxic effect in healthy peripheral blood mononuclear cells in healthy donors [66]. For pateamine A, assays were performed on JJN-3 multiple myeloma cell viability, and its $IC_{50}$ was determined as 2 nM [54].

The activity profile of these inhibitors has been thoroughly studied, however, their structural characterization while in complex with eIF4A is lacking. Apart from rocaglamide bound to RNA, no structures of other inhibitors bound to RNA and eIF4A have been determined [62]. Although NMR structural studies have been performed for hippuristanol, its exact mechanism is still unclear [50]. Obtaining structures of these inhibitors bound to eIF4A would provide a better understanding of eIF4A inhibition and potentially allow further optimization of the chemical structure for increased inhibitory potency.

## 1.6 Structural research

Crystallization of the entire eIF4F complex has been unsuccessful due to its size, but some success has been achieved in crystallizing partial fragments [67]. For example, only partial domains of eIF4G interacting with eIF4A and eIF4E have been structurally characterized [68, 69]. However, these structures of the complexes did not include RNA, despite findings which indicate eIF4G is able to interact with RNA [70].

Multiple structures of eIF4A have been published, from both yeast and human [71]. Initially, two structures, of the yeast NTD were published, allowing a structural understanding of the ATPase domain [71, 72]. One of these studies also obtained a crystal of full-length yeast eIF4A, however

only the NTD domain could be resolved in the electron density map [72]. They were subsequently able to clone only the NTD and crystallize the segment by itself [72]. Following this, a structure of the yeast eIF4A CTD was published [73]. Based on the previously reported conditions, they were able to crystallize and build a full-length structure of yeast eIF4A [73]. These findings provided information on the interactions between the two domains when not engaged with RNA [73]. As shown in the figure below (Figure 7), the two domains have no interaction with each other in the open state (i.e. not bound to RNA), resulting in a dumbbell shaped structure, with two separate domains connected by a short linker sequence [73].

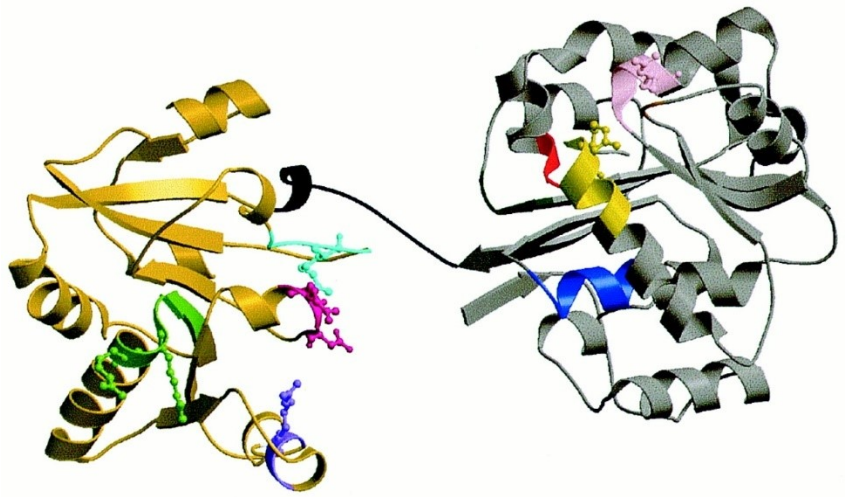

**Figure 7 –** Full length structure of eIF4A. N-terminal domain and C-terminal domain are colored in grey and yellow respectively with the linker in black. Other conserved sequences are individually colored. NTD domains are colored as follows, Motif I (walker A) is blue, motif Ia is yellow, motif Ib is pink and motif II (DEAD) is red. C-terminal domain conserved motifs are colored as follows: motif IV, green; "conserved R" motif, purple; motif V, magenta; motif VI, cyan. Figure 7 taken from Caruthers, et al. [73]

Using the information provided by the structure, researchers were able to theorize how eIF4A would interact with RNA, by comparing it with other helicase structures that had been crystallized with RNA. [73]. More recently, full length yeast eIF4A was crystallized with the MIF4G domain of eIF4G (displayed in Figure 8) [74]. This structure provided information of how the subunits of the complex interact with one another [74]. Using this structure as a basis,

other researches have further theorized that eIF4G functions as a clamp, and when in complex with eIF4A, maintains it into a closed form [75]. This closed conformation does not restrict RNA or ATP binding [75].

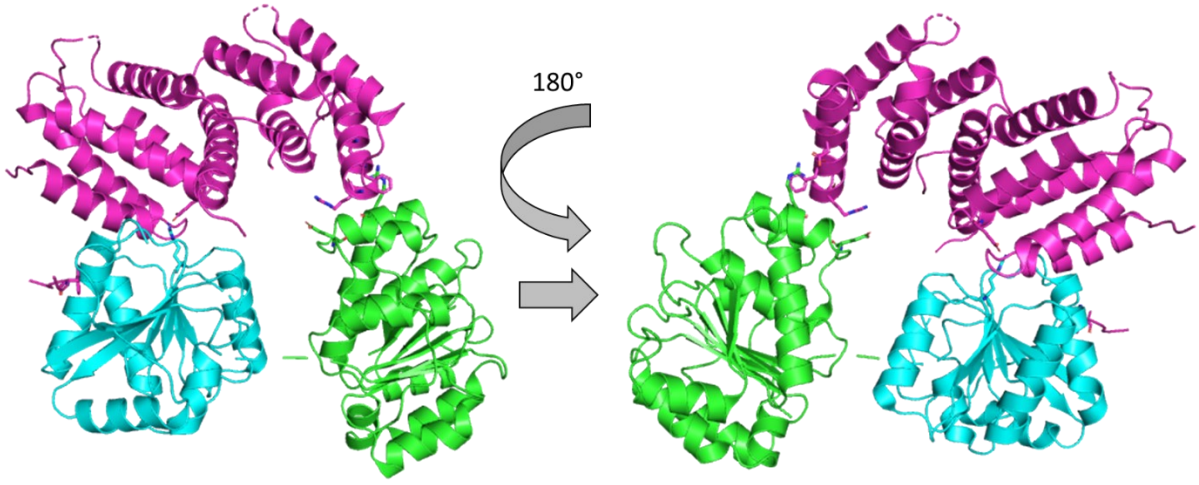


**Figure 8 –** eIF4A interacting with eIF4G domains. eIF4A CTD (colored green) and NTD (colored cyan) both interact with eIF4G (colored purple), allowing eIF4G the ability to fix the relative orientations of eIF4A domains to each other. Figure 8 created using data from Schütz, et al. [74]

Although both the yeast and human eIF4A share around 65% identity in sequence, they have substantial differences [76]. Expression of mouse eIF4A (all mammalian eIF4A has high similarity) in yeast was reported to be unable to support protein synthesis both in vivo and in vitro [77]. Both yeast and mouse eIF4A were also shown to have different affinities for RNA. Yeast eIF4A ATPase activity was much higher when in presence of double-stranded RNA, whereas mouse eIF4A had higher activity with single-stranded. Yeast eIF4A seems to prefer a 5' sequence overhang in translating sequences, whereas mouse eIF4A had no difference in activity with 5' or 3' [67]. Crystal structures of eIF4A from human include, one full-length structure of eIF4A with PDCD4, one NTD structure and two recently published structures with inhibitors, one containing sanguinarine and the other containing both rocaglamide and RNA [62, 78, 79]. The initial structure of PDCD4 with eIF4A allowed a better understanding of how inhibition of

the enzyme occurs. PDCD4 competes for the same interface eIF4A uses for RNA binding, and as such is able to sequester eIF4A and prevent mRNA translation [78]. The NTD structure was the result of a comparative study which crystallized the DEAD domain of various helicases [79]. The sanguinarine structure is the most recent structure, which provided information of how the ligand inhibited eIF4A. Unlike hippuristanol, which NMR studies provided evidence of interactions with both NTD and CTD, sanguinarine interacts exclusively with the NTD [47]. Using the previously crystallized NTD construct, researchers were able to co-crystallize sanguinarine with the NTD [47]. Sanguinarine was found to bind to the NTD in a position that partially interacts with ATP (when compared with eIF4AIII), resulting in the prevention of the formation of the closed conformation of eIF4A with RNA (as demonstrated in Figure 9) [47].

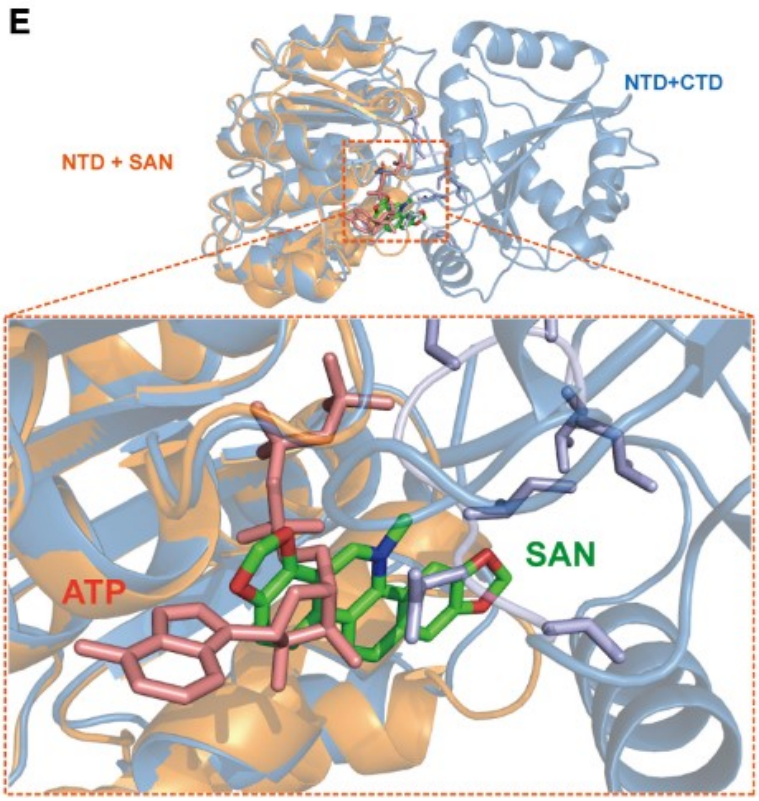


**Figure 9 –** Sanguinarine binding to eIF4A. eIF4A NTD structure with sanguinarine bound (colored orange) compared with the full length eIF4AIII structure with AMPPnP and RNA bound (colored blue). Sanguinarine results in the ATP binding site blocked and is unable to enter the closed conformation with RNA. Figure 9 taken from Jiang, et al. [47]

The rocaglamide structure, is particularly interesting as it is the first structure of eIF4A with a ligand and with RNA, providing structural information on both rocaglamide inhibition and how eIF4A interacts with RNA [62].

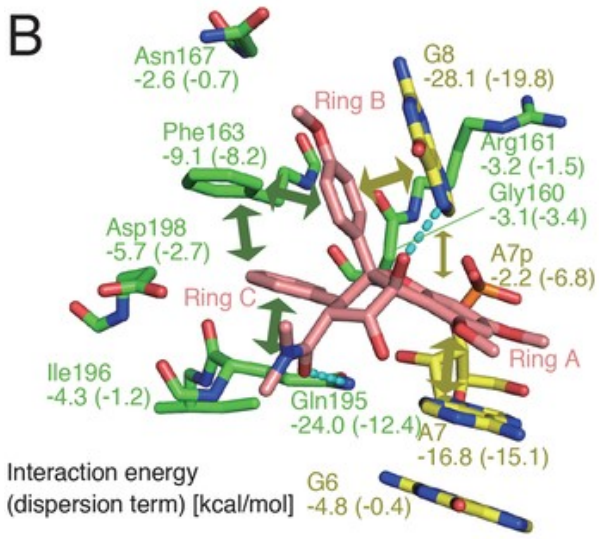


**Figure 10** – Rocaglamide-binding pocket in eIF4A. Rocaglamide is colored in red, RNA in yellow and eIF4A residues in green. Drug interactions with both RNA and protein involve pi-stacking. Interactions include both face to face and edge to face. Figure 10 taken from Iwasaki, et al. [62]

Rocaglamide is able to pi-stack with both RNA and eIF4A residues (as shown in Figure 10), resulting in the higher affinity of eIF4A for RNA [62]. With the structural data, researchers were able to rationalize why poly-purine RNA is targeted over poly-pyrimidine RNA. The phenyl ring of rocaglamide can pi-stack with the larger purine rings, which allows a stable interaction [62]. If the RNA base was replaced with a pyrimidine, the pi-stacking interaction is less complete and likely weaker [62]. The RNA is bent in the same manner as other RNA helicase structures with RNA, suggesting that the drug-free interface is similar [62].

## 1.7 Rationale of this study

Although much research has been performed in eIF4F function and regulation, its structural characterization is still incomplete. As an important subunit for the activity of eIF4F, eIF4A holds much promise in potential anti-cancer treatments. However, it lacks research in structural characterization with inhibitors. Only the structure of rocaglates with RNA has been obtained from all identified inhibitors. This study will attempt to obtain structural data of other inhibitors

with eIF4A like MZ735, which we obtained from a collaborator (Dr. Hull and Dr. Romero from Baylor University, Texas) and Hippuristanol. These results will provide further insight on other modes of inhibition for eIF4A and help guide the development of improved anti-cancer inhibitors.

# 2 Objectives

The aim of this research is to structurally characterize inhibition of eIF4A with hippuristanol and MZ735 to elucidate the mechanism of action of these compounds and to provide potential structural information for drug optimization. The hippuristanol could be potentially crystallized in complex with only the CTD of the protein (which has already been previously crystallized using yeast), as the NMR data shows contacts with mostly the CTD. Pateamine A also inhibits eIF4A with RNA. Using the same conditions rocaglamide was crystallized under, we might obtain a structure with pateamine A. Although the quantity of pateamine A we were able to obtain was limited, MZ735, an analog of pateamine A, was able to be synthesized by collaborators in large enough amounts for crystallization. This would potentially allow conclusions on pateamine A-like compound binding.

# 3 Methodology

## 3.1 Cloning

Initial yeast 4A CTD plasmids were obtained from Dr. Jerry Pelletier's laboratory. The construct was derived from the previously published structure [73]. The yeast construct was engineered with a hexa-histidine sequence with a SUMO solubility tag followed by yeast eIF4A residues 231-395. 4A yeast sequence was cloned into the pSMT3 plasmid using primers purchased from Biocorp. Another construct of the human eIF4A full length was provided by Dr. Jerry Pelletier,

with the first 19 amino acids removed (previously used in the crystallization in conjunction with PDCD4 [78]) in the pet15b plasmid. The construct was designed with a hexa-histidine sequence followed by a cleavage site with the human eIF4A residues 20-406.

eIF4A was cloned from other species through cDNA libraries. Chicken and Drosophila were chosen, which provided a larger screen of hits due to differences in sequence identity. Mammals have 100% identical eIF4A, whereas chicken eIF4A has 97% similarity and fly has 88% similarity compared to the human eIF4A. Constructs were built similarly as before: hexa-histidine sequence with a SUMO solubility tag followed by eIF4A, in which the eIF4A was the sequence of either chicken or drosophila, full length or CTD portion only.

## 3.2 Expression and purification

Expression of proteins was carried out in E. coli. Protocols were taken from the previously published purification [73]. pSMT3-eIF4A was transformed into BL21 (DE3) competent cells. Starter cultures were grown overnight at 37 °C in 20 mL (per 1 litre of culture) of LB media with kanamycin. Starter culture samples were transferred into flasks of 1 L LB with kanamycin and grown until $OD_{600}$ reached 0.6. Expression was induced with 1 mM IPTG for 4 hours at 37 °C. Cells were harvested through centrifugation at 4000 rpm (3993xg). Cells were pelleted and resuspended in 300 mM NaCl, and 20 mM Tris pH 7.4. Samples were lysed by sonication. Cell lysate was then centrifuged at 19000 rpm (43667xg), for 40 minutes. Once pelleted, free flowing nickel-NTA beads were added (2 mL of slurry per 50 mL of cell lysate). Samples were incubated on a rotating platform for an hour at 4 °C. Beads were then pelleted at 2000 rpm (1862xg). The supernatant with beads was then applied to a glass column and washed with 300 mM NaCl, 20 mM Tris pH 7.4, 3 mM imidazole. Elution was carried out in 300 mM NaCl, 20 mM Tris pH 7.4, 300 mM imidazole solution (3 mL of elution buffer per 2 mL of initial bead slurry). The His6-

SUMO tag was cleaved with ULP (purified in the lab by colleagues) overnight, while dialyzed in 100 mM NaCl and 20 mM Tris pH 7.4 buffer at 4 °C. The sample was then applied to a nickel-NTA column, with the flow-through collected. The sample was then applied to a Superdex s75 gel filtration column and the eluting fractions were collected and concentrated.

For the full length eIF4A, we followed a modified version of the protocol provided by Dr. Pelletier to remove possible additives that might be detrimental for crystallization. pET15b-His6-3C-eIF4A was transformed into BL21 (DE3) competent cells. Starter culture was grown overnight at 37 °C in 20 mL (per litre of culture) of LB media with ampicillin. Culture samples were transferred into 1 L of LB with ampicillin and grown until $OD_{600}$ reached 0.6. Expression was induced with 1 mM IPTG for 4 hours at 37 °C. Cells were then pelleted at 4000 rpm (3993xg) for 20 minutes. Cells were resuspended in sonication buffer (20 mM tris pH 7.4, 10% glycerol, 0.1 mM EDTA, 200 mM KCl, 0.1% Triton X-100 and 3.4 mM Beta-mercaptoethanol) at 30 mL/L of culture. Cells were lysed by sonication. Lysate was pelleted at 19000 rpm (43667xg) for 40 minutes. Imidazole was added for a final concentration of 20 mM. Samples were incubated with nickel-NTA beads (2 mL of slurry per 50 mL of cell lysate) for an hour on a rotating platform at 4 °C. Beads were pelleted at 2000 rpm (1862xg). The supernatant with beads was then applied to a glass column and washed with two different wash buffers (20 mM Tris pH 7.5, 10% glycerol, 0.1 mM EDTA, 800 mM KCl, 20 mM imidazole and the second buffer containing 300 mM KCl) and eluted with 20 mM Tris pH 7.5, 10% glycerol, 0.1 mM EDTA, 300 mM KCl, 2 mM DTT, and 0.2 M imidazole. 1 mg of PreScission protease was added for each 10 mg of purified eIF4A (quantified by UV absorbance at 280 nm), to remove the histidine tag. Samples were dialyzed overnight in 1L of A100 buffer (20 mM Tris pH 7.5, 10% glycerol, 0.1 mM EDTA, 100 mM KCl) at 4 °C. Digested protein sample was loaded onto a Q-Sepharose

column (washed with A100 solution beforehand) and eluted using A500 buffer (500 mM of KCl instead of 100 mM), with the main peak collected. The collected fraction of eluted protein was then incubated with 1 mL of glutathione-agarose beads for one hour to remove the protease. Beads were applied to a glass column and the flow-through was collected. Finally, the sample was run on a Superdex gel filtration column (s200) with 20 mM Tris pH 7.4, 100 mM KCl as buffer.

### 3.3 Complex Formation

Samples with hippuristanol were originally mixed in a 2:1 molar ratio with purified eIF4A. This ratio is the same used in the previously performed NMR studies, where peak shifts were demonstrated [36]. The inhibitor was gradually added while mixing on a rotating platform at 4 °C. For alternative mixes, 0.1% Triton-X was added, and in order to minimize DMSO (in which the inhibitor was dissolved), samples were first diluted by a factor of 10 with buffer and then hippuristanol was added and mixed for an hour. Samples were concentrated back to the initial volume.

For pateamine A analog MZ735, samples were prepared using the same ratios described in the crystallization of rocaglamide bound eIF4A by Iwasaki et al. [62]. Briefly, concentrated eIF4A at 20 mg/mL was supplemented with 10-mer $r(AG)_5$ RNA (purchased from IDT) at a 3:1 molar ratio, AMP-PNP at a 16:1 molar ratio, and MZ735 at a 2:1 molar ratio. The complex was then diluted with gel filtration buffer such that the final protein concentration was 3 mg/ml. $MgCl_2$ was finally added at a concentration of 5 mM.

## 3.4 Crystallization Trials

Crystallization trials were carried out with commercial screens from Qiagen. These included the Classics I, Classics II, ProComplex, PEGs I, PEGs II, JSGC+ and Ammonium Sulfate suites. Other custom screens were made with the Formulatrix Formulator Screen Builder robot. Commercial screens trials were conducted in sitting drops at 2/5/10 mg/ml concentrations in 96 well plates prepared using the Formulatrix NT8 Drop Setter. Crystals were then further optimized in hanging drop screens with 24 well plates. Seed stock was prepared through harvesting old crystals mixed with 50 microlitres of old well solution. Crystals were vortexed for a minute and subsequently diluted by 100 and 10000. Seeding stock was applied using a hair to brush seeding solution into drops.

## 3.5 X-ray Crystallography

Crystals with PEG-based conditions were cryoprotected with 20% glycerol. Crystals from salt-based conditions were cryoprotected with 2 M sodium malonate solution. Crystals were screened using a Bruker D8 Venture diffractometer. After confirming diffraction, crystals were sent to the Canadian Light-Source (CLS) synchrotron in Saskatoon, where full data were collected with the 08ID-1 beamline and the Pilatus3 S 6M X-ray detector.

## 3.6 Structure Determination

Diffraction data were processed with the HKL2000 software. Data were indexed, integrated, and scaled using auto-corrections. This dataset was then used for the molecular replacement function in Phenix using the previously solved yeast eIF4A CTD structure (PDB ID: 1FUK [73]) for the hippuristanol dataset and the human eIF4A with rocaglamide structure (with rocaglamide removed) (PDB ID: 5ZC9 [62]) for the MZ735 dataset as search models in Phaser. The structures were manually built using Coot and refined in Phenix using these options: XYZ

coordinates, individual B-factors, Translation – Libration – Screw (TLS) parameters, x-ray/stereochemistry and x-ray/ADP weights optimized [80]. For the MZ735 structure, AMPPnP and RNA were kept in the molecular replacement model, and MZ735 was built using difference electron density. Structure figures were produced using Pymol.

### 3.7 Differential Scanning Fluorimetry

Samples were prepared in a RT-PCR plate. Protein samples were mixed with compound and diluted. Mixture was aliquoted into the plate and then Protein Thermal Shift dye from Fisher was added. Heating program started at room temperature and gradually increased up to 99 °C in the span of an hour, using an Applied Biosystems One Step Plus Real-Time PCR system.

### 3.8 Mass Spectrometry

10 ug of samples were applied to a PLRP-S reverse-phase chromatography column and analyzed on a Bruker ion trap mass spectrometer.

## 4 Research Findings

### 4.1 Hippuristanol

Yeast eIF4A CTD was initially cloned from previously obtained plasmids and integrated into the pSMT3 plasmid. Purification was carried out and crystal screens around the specified conditions were tested to confirm previous findings. Crystals were successfully replicated, however, due to the presence of zinc in the crystallization condition, previous conditions were unable to be used for co-crystallization or soaking. It was previously demonstrated that the inclusion of zinc catalyzes the conversion of hippuristanol into an inactive compound [81]. This occurs through the conversion of C22, from R to S chirality, which was previously mentioned as critical for its activity [36].

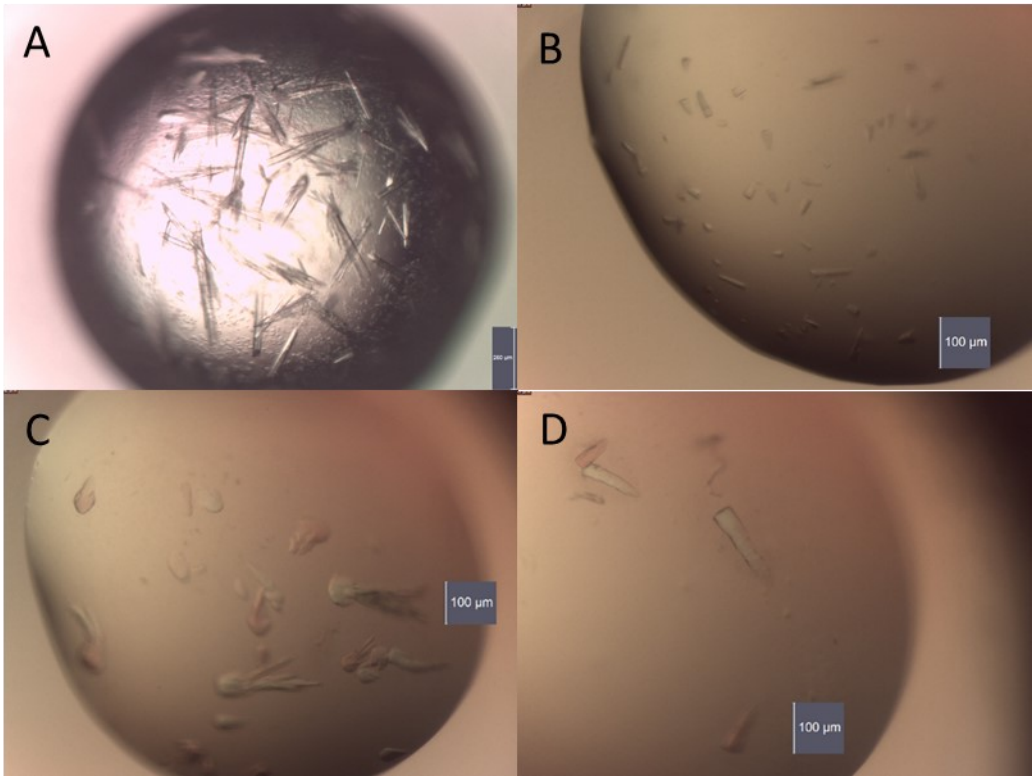


**Figure 11** – Obtained eIF4A CTD crystals. A contains crystals initially obtained with zinc. B, C and D are of crystals obtained using commercial screens and optimization.

Since the crystal structure itself contained a molecule of zinc, zinc seemed integral for obtaining that specific crystal form. Magnesium, calcium, and nickel were then used as potential replacements for the divalent ion. These were unsuccessful. Other crystal forms were obtained using the commercial screens (crystals shown in Figure 11). From those screens, several hits were obtained, and then optimized. Those crystals obtained from the optimization conditions underwent data collection at the CLS synchrotron. One set of data was very poor, only diffracting to a resolution of 4 Å. The other data set extended to 2.1 Å, however, due to the presence of ice rings, some of the data were contaminated. It was then processed with HKL2000 resulting in a mediocre dataset with low-resolution completeness under 70%, even though the final resolution limit of 2.39 Å was acceptable. The structure was solved by molecular replacement using Phaser in Phenix, with the previously solved yeast CTD structure as a starting

model (PDB ID: 1FUK) [73]. The crystal structure is displayed in Figure 12. Although a shift in one alpha helix (residues 295 – 307) was observed, the structure did not appear to contain hippuristanol.

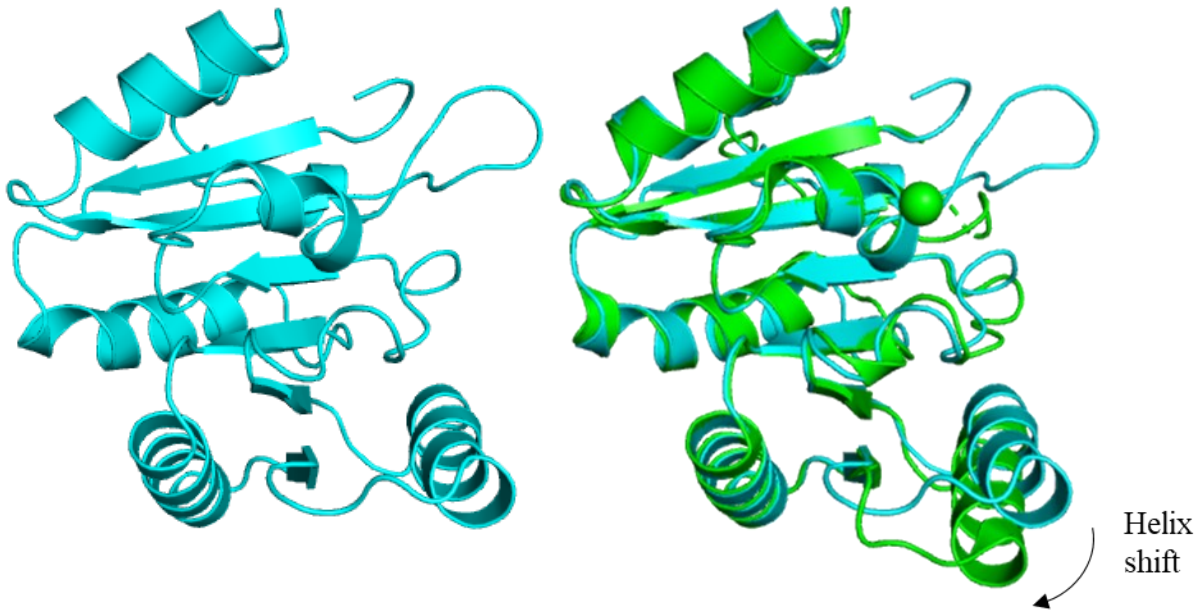


**Figure 12** – eIF4A CTD crystal structure. On the left is the crystal structure obtained in blue. On the right is a comparison with the previously determined apoprotein eIF4A CTD in green. Note the shift in the lower alpha helix.

Other eIF4A constructs were cloned from cDNA libraries, to attempt crystallization of homologs. Human, chicken, and drosophila were chosen, as all mammalian species have very close similarity. eIF4AII was also cloned. Human constructs were initially full-length, however at the suggestion of Dr. Pelletier, 19 amino acids were excluded from the NTD. This was to emulate the full-length protein which was previously crystallized with eIF4A with PDCD4 [78]. Human full-length, human CTD and full length Δ19 were all screened, both apo and mixed with hippuristanol, yielding no hits. To conserve hippuristanol, the other constructs from fly and chicken were not screened with hippuristanol, but only the apo protein. This also yielded no hits in the commercial crystallization screens.

As we obtained no crystals with other species, priority was placed back on yeast eIF4A crystals. The initial stock of hippuristanol began precipitating after thawing. Instead an alternative way of mixing smaller volumes of protein and hippuristanol sample were attempted. When using a detergent to solubilize hippuristanol a new profile of hits in the commercial screens was obtained. When mixing lower volumes, the same new set of hits was obtained. These new crystal hits were unable to be reproduced outside the commercial screens. Solutions in hanging or sitting drops in the 24-well plates produced no crystals, nor any screens made using the Formulatrix Formulator robot. Commercial screens were once again attempted while searching for another potential lead and previously recorded hit resulted in higher quality crystals. Using the home source X-ray Bruker, a 1.3 Å dataset was able to be obtained, with a structure containing the same alpha helix movement (residues 295 – 307). However, in this structure there was also no addition electron density indicating the presence of hippuristanol. Thus, hippuristanol was unable to be co-crystallized with eIF4A.

## 4.2 MZ735

MZ735 crystallization began by attempting to replicate previously published human eIF4A with rocaglamide crystals. Similar conditions were used [80 mM HEPES (pH 7.5), 1120 mM tri-sodium citrate, 100 mM ammonium sulfate, 20 mM Bis-Tris (pH 6.0), 0.2% (w/v) polyethylene glycol 3,350, and 40 mM lithium chloride] with poly-purine RNA, AMPPnP and 1, 2, or 4 mg/ml protein concentrations [62]. This yielded no crystals or precipitation, so higher concentrations were tested. When crystals still did not develop, commercial screens were tested. The protein buffer (NaCl, Tris pH 7.4, Triton X-100 and glycerol) was swapped after commercial screens resulted in no hits and replaced with a more minimal buffer (only 100 mM NaCl and 20 mM Tris pH 7.4).

To confirm the binding of the drug, differential scanning fluorimetry (DSF) assays were performed.

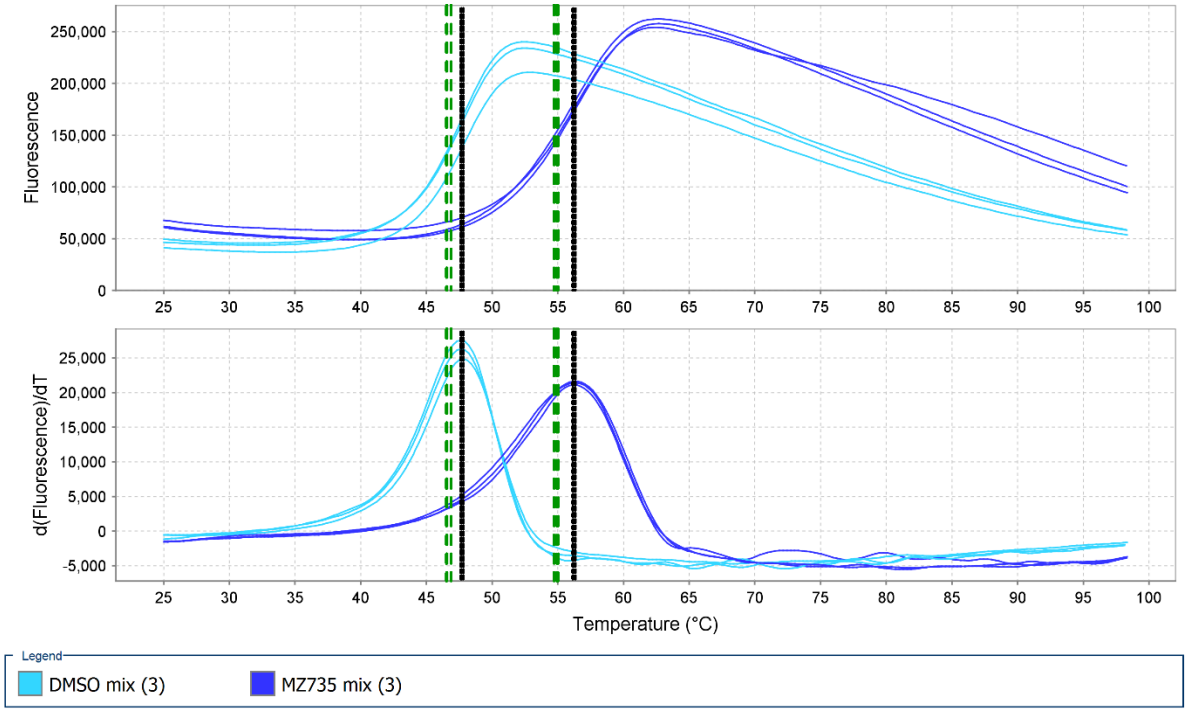


**Figure 13** – Increase in eIF4A melting point with the addition of MZ735. Dark blue indicates MZ735 addition and light blue indicates the sample with DMSO. Green dotted line represents the Boltzmann calculated Tm (54.9 ± 0.1 to 61.1 ± 0.1 °C), and black dotted line is the derivative calculated Tm (55.7 ± 0.1 to 62.2 ± 0.1 °C). In either case the melting temperature increases about 6 °C.

An increase in the melting temperature of eIF4A was observed upon the addition of MZ735 (as shown in Figure 13). This would provide evidence that MZ735 is indeed interacting with eIF4A, as its addition stabilizes eIF4A.

The initial crystallization screens also lacked a Mg ion that is present in the 4A-rocaglamide structure. This was rectified by adding 5 mM $MgCl_2$ afterwards. With the addition of magnesium, multiple hits were obtained from the commercial screens, with most hits being in ammonium sulfate containing conditions. Further optimization was carried out after grouping similar hits (one with just different ammonium sulfate concentrations and the other with PEGs).

The commercial ammonium sulfate screen was tested, to determine the effects of different salts. However, hits remained generally similar, despite the presence of different salts. Another 24-well screen was set up using different salts. The crystals obtained were of a shape not conducive to data collection, consisting of clusters of thin plates (as seen in Figure 14).


**Figure 14** – Initially optimized crystal hits. All conditions for crystals contained ammonium sulfate at different pHs at a protein concentration of 5 mg/ml. A is 2.4 M AmS at pH 8.5, B is 2.2 M AmS at pH 6.5 and C is 2.4 M AmS at pH 6.5.

Micro-seed stock was prepared from these crystals and used in subsequent screens. Crystal samples were screened at the MUHC (McGill University Health Center) on a Bruker D8 Quest diffractometer and samples with diffraction were sent to the CLS synchrotron. Although the crystal screened contained multiple stacked crystals, data were collected from a uniform portion. Upon indexing, integrating and scaling data through HKL2000, a unit cell and space group comparable to the rocaglamide structure previously published was obtained [62]. The rocaglamide structure was used for molecular replacement (with the rocaglamide removed) and confirmed the presence of RNA and AMPPnP in the sample. Due to the low resolution of the data (around 3.9 Å), the ligand could not be placed, however, weak electron density was present around the rocaglamide binding site, which might possibly be the MZ735.

The assays carried out by Dr. Jerry Pelletier's lab indicated that inhibition by pateamine A was irreversible, suggesting that the compound was bound covalently. Using the tentative structure, the only possible residue in contact in the electron density would be glutamine 195. Mass

spectrometry was performed to determine if inhibitors bound covalently to the protein. Mass spectrometry data (visible in Figure 15) confirmed the mass of the protein correctly (measured mass was 44291.83 Da, calculated mass is 44288.99 Da). The other sample which contained a negative control CMLD012612 (an amino-rocaglate [derivatives of rocaglates] which binds non-covalently [58]) and MZ735 (with RNA, $MgCl_2$ and AMPPnP) failed to shift the mass spectrometry peak, indicating non-covalent interactions.

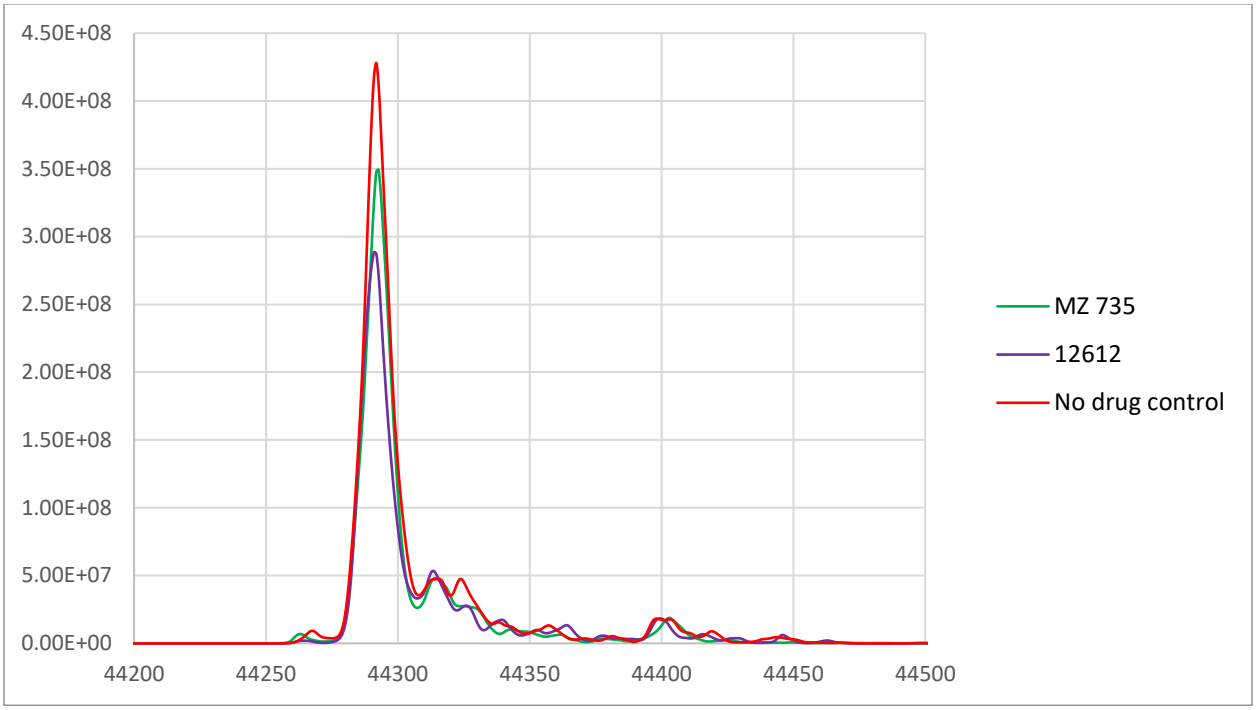


**Figure 15** – Mass spectrometry data of eIF4A samples. Red line was the data obtained for protein incubated with DMSO, while the light green was incubated with MZ735. Purple line is for the drug which interacts non-covalently. There was no change in the main peak (44291.83 for all 3 peaks) upon incubation with MZ735.

Other screens were repeated with finer ranges of pH and precipitant concentration to optimize singular crystals. More crystals were collected and sent to the CLS synchrotron after screening. Data were processed using HKL2000 and the same previously used structure was chosen again for molecular replacement. The resulting structure was built at a final resolution of 2.9 Å (shown

in Figure 16). Electron density was observed for a ligand and indicated the presence of MZ735 (Figure 17 displays the density before placement).

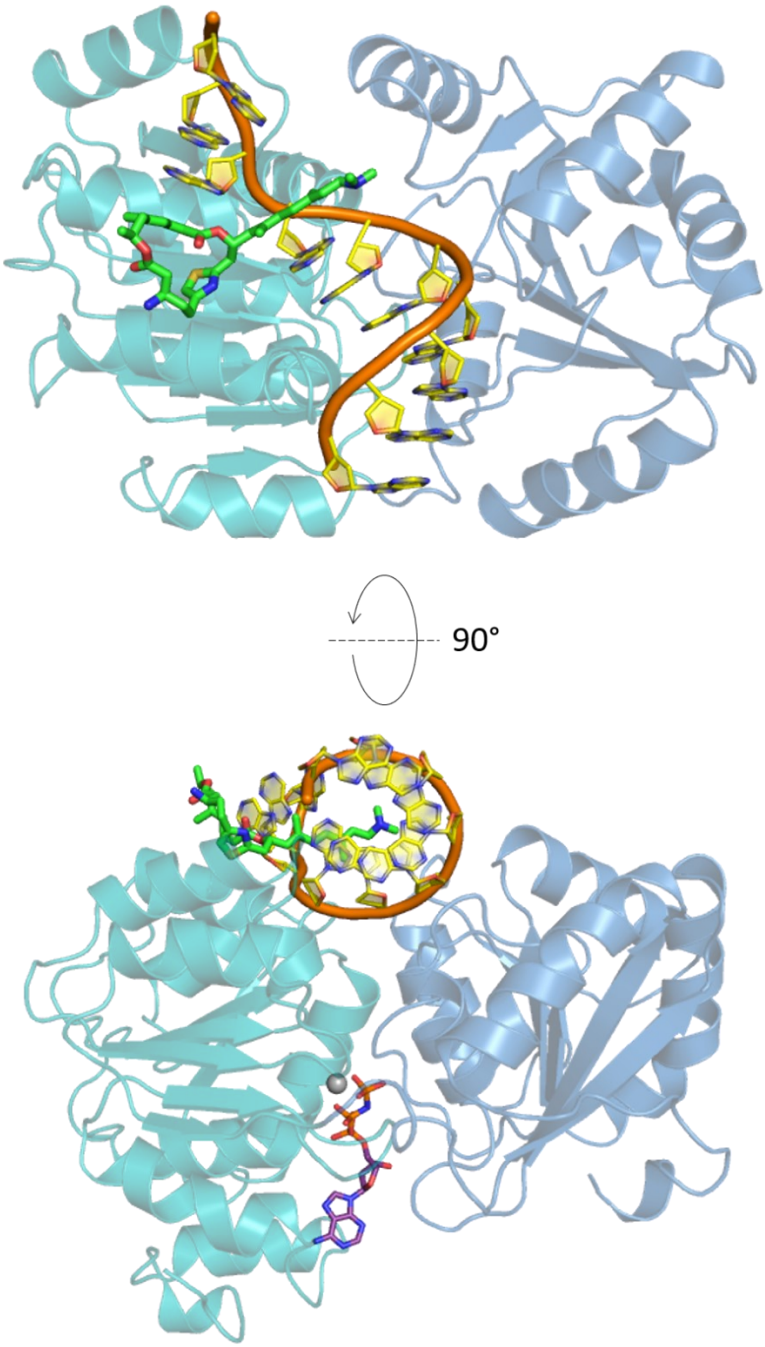


**Figure 16** – Overview of the obtained eIF4A structure with RNA and MZ735 bound. eIF4A is blue (with the NTD teal and the CTD in navy), RNA in yellow, AMPPnP in purple, Mg2+ ion in grey and MZ735 in green.

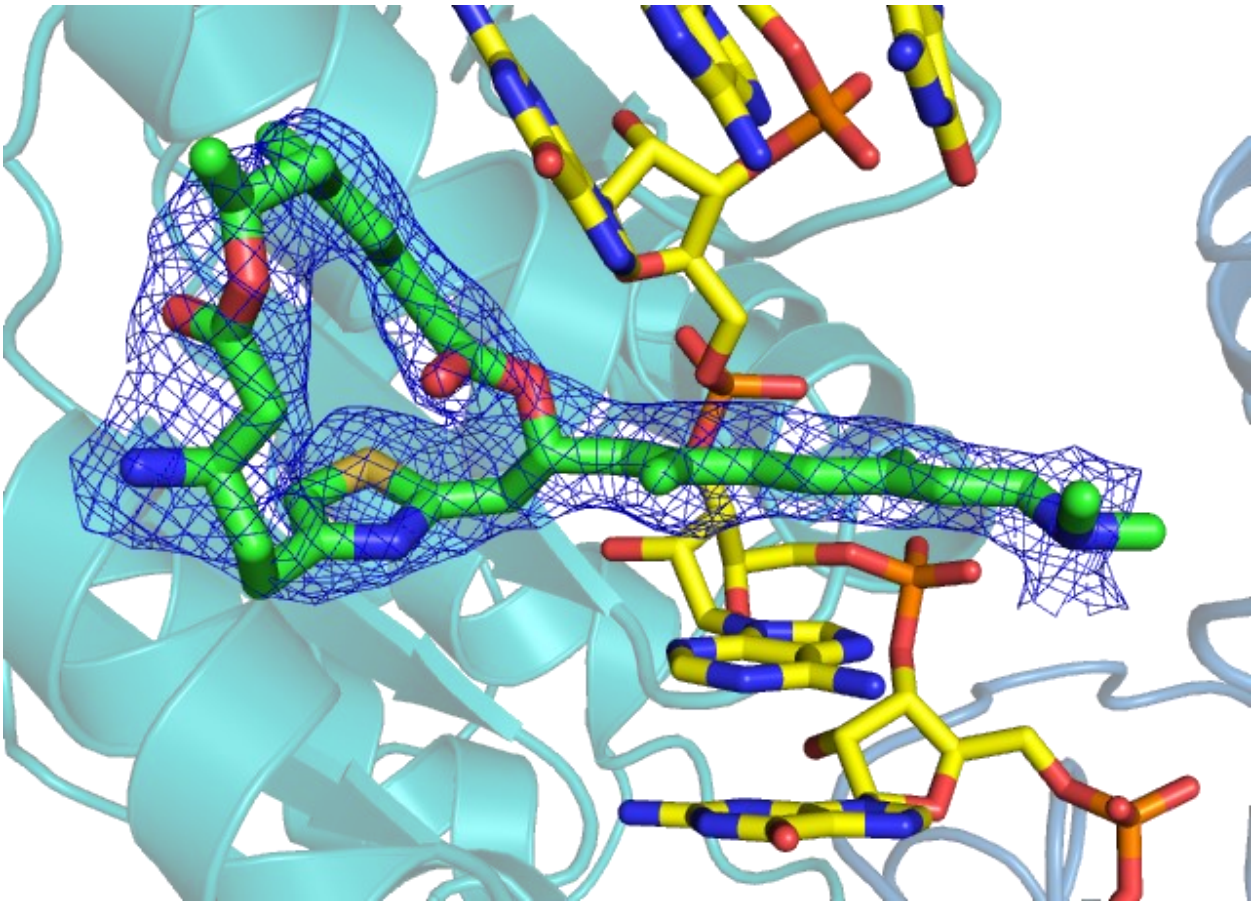

**Figure 17** – One sigma electron density around MZ735. Electron density (2Fo-Fc map at 1.0 sigma) around the potential MZ735 binding site.

eIF4A and RNA overlap with their positions in the rocaglamide structure. MZ735 is positioned in the same pocket as rocaglamide, inducing the same kink in the RNA strand. This is maintained through pi-interactions. The trienyl amine arm interacts with both the lower base (Adenine 7) with a face to face pi-interaction, and the higher base with an edge to face interaction (Guanine 8). The E, Z-dienyl lactone portion of MZ735 also interacts with the upper base through face to face pi-stacking. In addition to these interactions with RNA, the macrocycle ring interacts with mostly the NTD of eIF4A. The thiazole ring pi-stacks with phenylalanine 163 above it and has hydrophobic interactions with glutamine 195 underneath it. A hydrogen bond between the C3-primary amide and aspartate 198 was also identified. All these interactions are labeled in Figure 18.

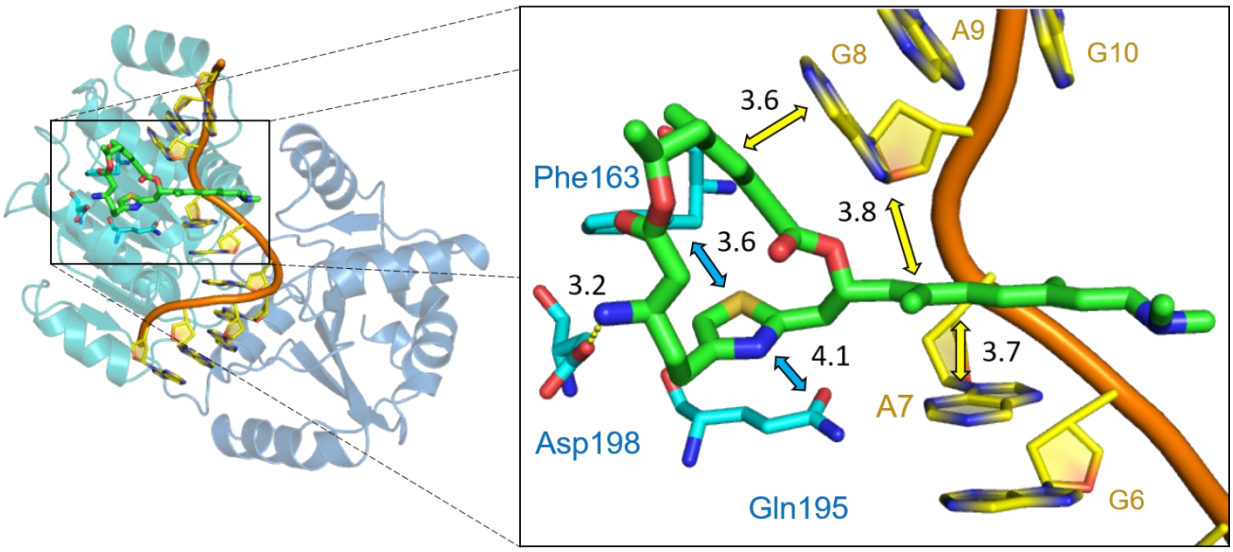


**Figure 18** – Distances between MZ735 and the protein with RNA bound. Arrows represent potential hydrophobic or pi-interactions (either face-face or edge-face). The hydrogen bond between aspartate 198 and the primary amine on the MZ735 ligand is also displayed through a dotted yellow line.

By inducing this kink in the RNA strand, MZ735 creates a stable interface between RNA and eIF4A, locking them together, impeding the scanning function of eIF4A.

# 5 Discussion

From the data obtained with the initial hippuristanol structure, we observed a significant shift in one of the alpha helices. However, it is uncertain if this is relevant, as hippuristanol does not appear to be present, when looking at potential binding modes from docking models using data from the NMR experiments (Dr. Jerry Pelletier, personal communications). The shifting of the alpha helix in question is most likely due to a crystal contact from aspartic acid 282 in the alpha helix with lysine 303, which could make this a crystallographic artifact (demonstrated in Figure 19).

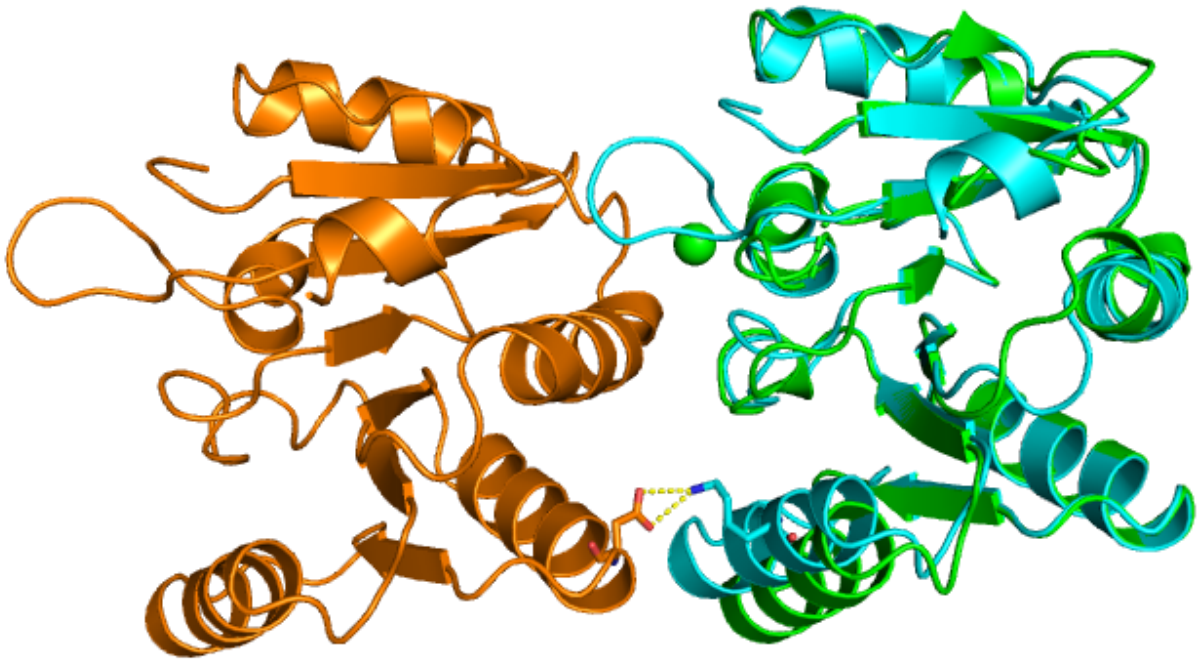

**Figure 19** – Potential crystal contact between eIF4A and another symmetry mate. Symmetry mate is colored orange with asp282 displayed as sticks. The alpha helix in the crystallized structure (colored cyan) appears to deviate from the previously crystallized structure (colored green) in the same direction of the crystal contact. The interactions between the two are shown using a yellow dotted line.

Examining the electron density, hippuristanol is not present in the structures we determined. It might be due to how hippuristanol interacts with the protein, resulting in a less favorable orientation for crystallization or perhaps the necessary saturation was not reached because not

enough ligand was bound. Potential research avenues from here would be to generate crystals using the previous conditions and then soak them in hippuristanol in attempts to insert hippuristanol in its binding site, use higher concentrations while mixing or undertaking co-crystallization with the full length yeast eIF4A which we were unable to clone, due to the lack of a yeast cDNA library. Although hippuristanol interaction is minimal with the eIF4A NTD, it might provide a structural interaction with hippuristanol, allowing it to be further stabilized in the binding pocket.

Examining the structure obtained with MZ735, we confirmed the presence of MZ735 and determined the interactions which would allow the ligand to bind to both eIF4A and RNA. The structure can then be compared with the previously crystallized structure with rocaglamide. The rings A, B and C in rocaglamide were previously identified as important for binding with eIF4A and RNA [62]. These rings all overlap with equivalent pi-systems in MZ735. Ring A overlaps with the trienyl amine arm, ring B overlaps with the diene portion of the main ring and ring C overlaps with the thiazole ring. This results in the ability for MZ735 to interact non-covalently with eIF4A and RNA in the same fashion that rocaglamide is able to, while having such a vastly different structure. Figure 20 provides a visual comparison of these overlaps.

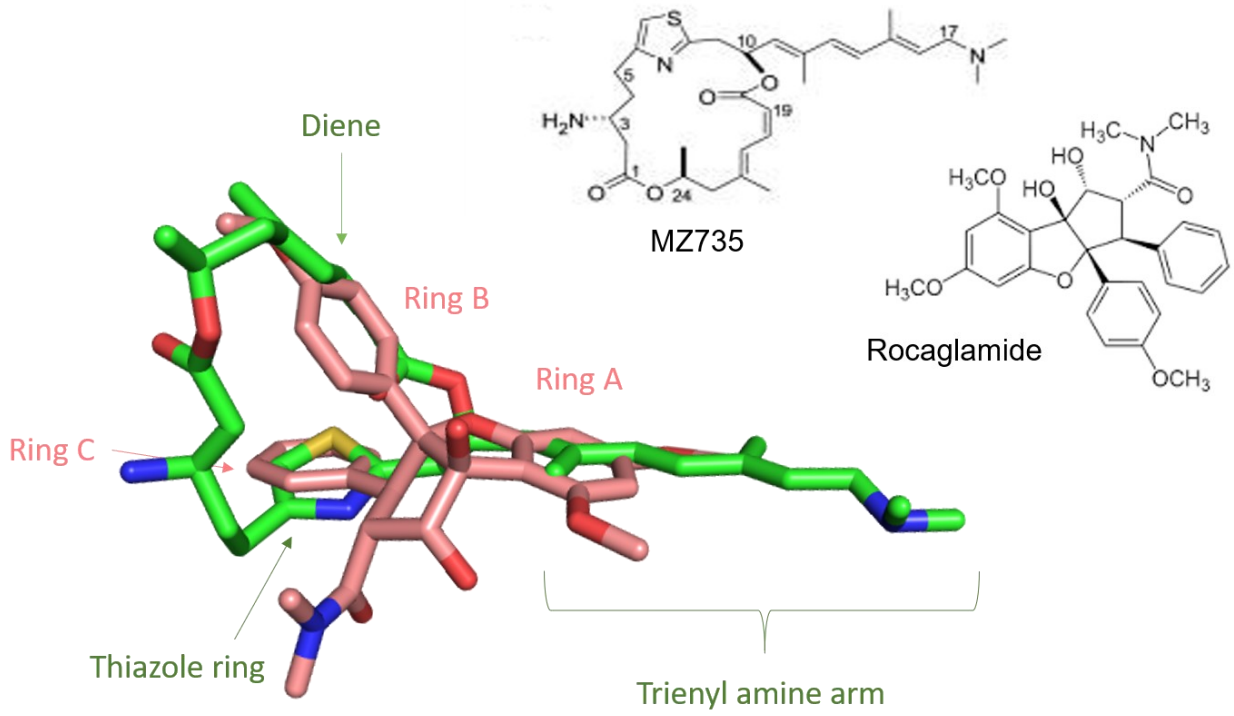


**Figure 20** – Overlap of MZ735 placement and rocaglamide. Positions of rocaglamide (colored pink) and MZ735 (colored green) compared through superimposing the previously published structure of eIF4A with rocaglamide. The three rings (A, B and C) which were previously identified as important for rocaglamide binding have equivalents in MZ735. Both ring A and B overlap with double bond pi-systems in MZ735 and the ring C in rocaglamide overlaps with the thiazole ring for MZ735.

This result would explain why rocaglamide resistant mutations share cross-resistance to pateamine A/MZ735 as mutations which impact these rings would affect both molecules (Dr. Jerry Pelletier, personal communications). The cross-resistant mutations specifically identified are ones that impact the phenylalanine and glutamine which interact with the ring C in rocaglamide or the thiazole ring for MZ735. This also confirms that MZ735 interacts with eIF4A non-covalently, which is further supported by the mass spectrometry data. This suggests that pateamine A binding should be reversible, its previous labeling as irreversible was potentially due to having such a strong affinity [35].

The interactions between MZ735 and eIF4A may bring information on other similar compounds and how they would potentially interact with eIF4A. Figure 21 displays the differences in structure between pateamine A and pateamine A-like compounds.

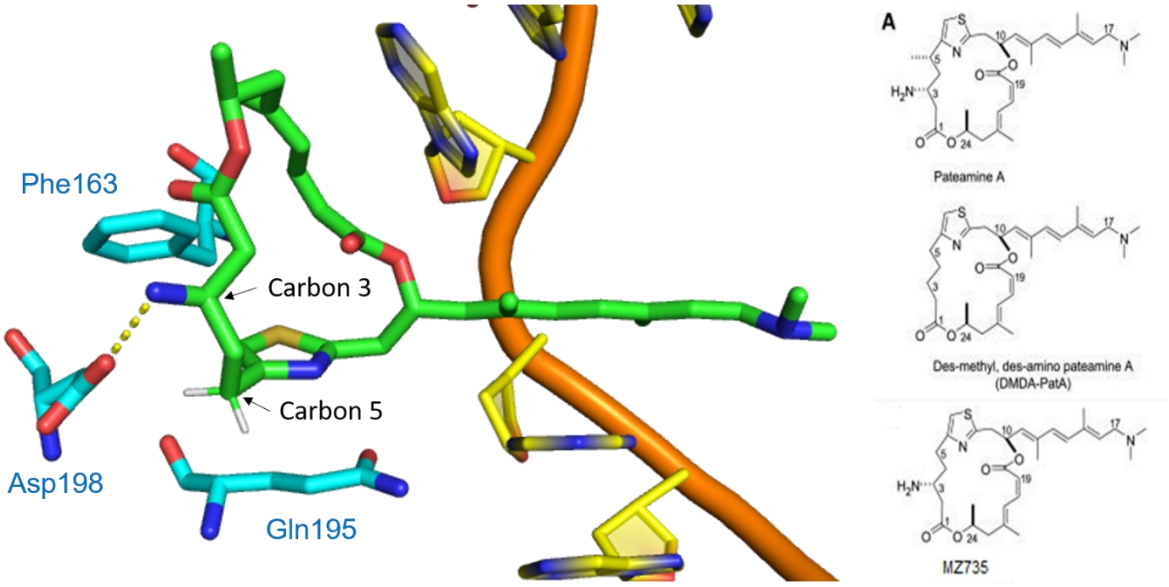


**Figure 21** – Differences in structure of pateamine A-based ligands. On the right are the structures of pateamine A (originally discovered to have anti-proliferative effects), DMDA-PatA (pateamine A analog which maintained its activity) and MZ735 (second generation analog synthesized through parallel synthesis). Carbon 5 and 3 are labeled on the structure on the left indicating where the differences between the ligands are present. The additional methyl group for pateamine A would replace the lower hydrogen indicated on the figure.

Possible reasons for the increased potency of MZ735 compared to pateamine A and DMDA-PatA can be determined through these structural discoveries. As previously noted, aspartate 198 was identified having a potential interaction with the primary amine on carbon 3 of MZ735. This interaction might help position the ligand in the binding pocket. The reason for the reduced potency of the DMDA-PatA may then be potentially explained as this amine is not present. The reason for the difference in affinities of MZ735 and pateamine A is still uncertain, the additional methyl group might interfere with glutamine 195, resulting in weakened hydrophobic interactions or disrupting the hydrogen bonds with the lower base. However, this would need to be further confirmed through a structure with pateamine A.

In terms of sites for potential SAR, the tertiary amine at the end of the arm of MZ735 does not interact with the protein. It does however interact with two water molecules forming, which in turn interact with the RNA bases underneath. A possible way to improve MZ735 potency could be to extend the arm by an extra carbon and might result in an interaction with aspartate 305 (site displayed in Figure 22). This could be further improved if the amine were modified into a secondary or primary amine, resulting in a potential salt bridge with the aspartate, which would make a stronger interaction. Previously in the SAR study of pateamine A derivatives, the length of this arm was not modified [65]. Researchers noted a loss of activity when modifying the rigidity of the trienyl amine arm through unsaturation of the carbon bonds. This may be explained by the loss of important pi-stacking interactions, identified earlier. The report also suggested that the N,N-dimethyl amino group might be optimized for stability or solubility of MZ735 in preclinical trials, which may also use this extra space demonstrated in the structure [65].

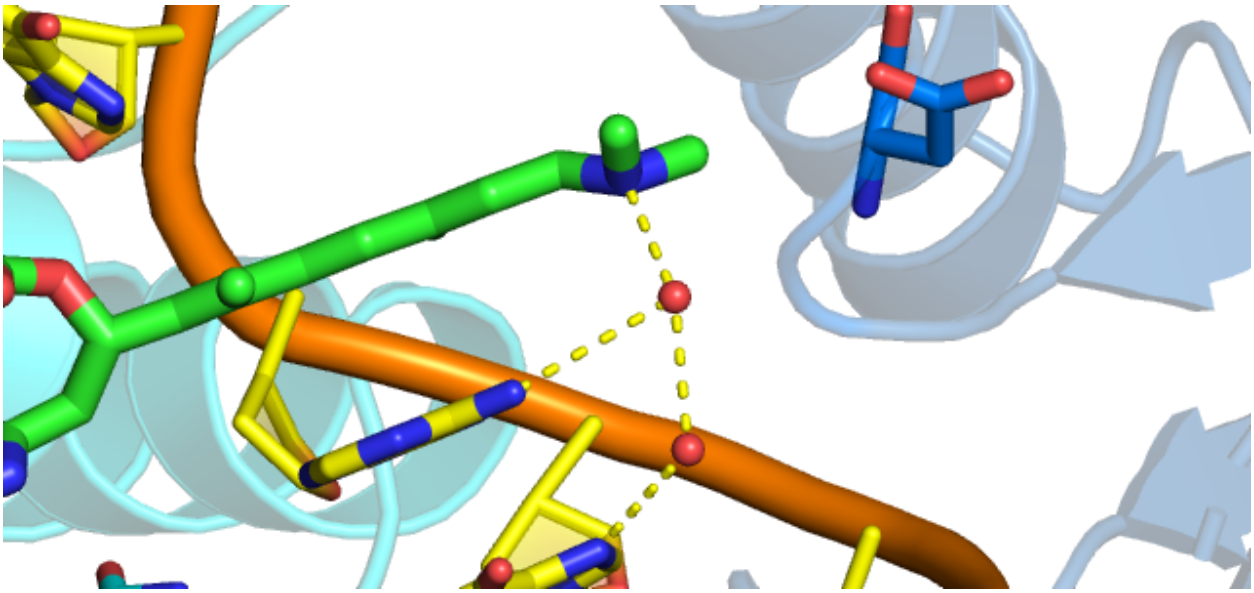

**Figure 22** – Potential SAR site for MZ735. The tertiary amine on the arm of the MZ735 does not interact with anything other than waters, which are displayed as red spheres (interactions are shown with yellow dotted lines). Aspartate 305 is shown as sticks for a reference in distance.

The suggested modifications on MZ735 would need to be tested to ensure that the changes are relevant and would provide more insight on the validity of our model. There might also be an explanation for the non-selectivity of RNA sequence with MZ735. Rocaglamide was demonstrated in the previous study to be unable to interact with pyrimidine residues due to the smaller bases and a hydrogen bond with purines also drove selectivity (which is not present in pyrimidines) [62]. On the other hand, MZ735 has been demonstrated to have no poly-purine bias through fluorescent polarization assays (Dr. Jerry Pelletier, unpublished data). In the structure we obtained, we modeled pyrimidine bases by replacing the current purine bases, and the extended pi system on the tertiary amine arm results in the smaller pyrimidine bases to remain in partial contact. Although it does not seem to align wholly, this might be due to using the purine structure. With actual pyrimidine basses the ligand might adjust. The differences in overlap may be observed in Figure 23.

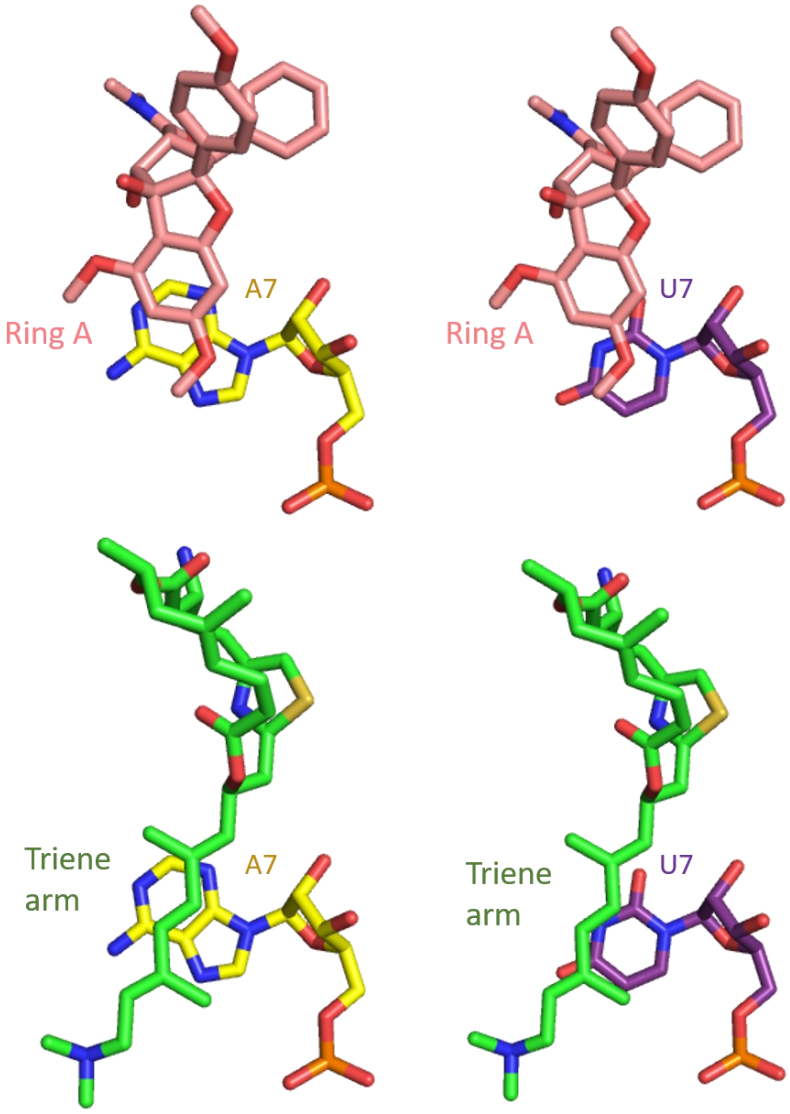


**Figure 23** – Binding differences between poly-purine RNA and poly-pyrimidine RNA, in respect to MZ735 and rocaglamide. Purine bases are labeled in yellow, while pyrimidine bases are purple. With rocaglamide, A7 overlaps wholly with the rings of rocaglamide, however the distance becomes too small when replaced by U7. MZ735 on the other hand maintains a closer contact with U7 with its longer reach.

Rocaglamide was presented as an inhibitor which would allow the targeting of specific poly-purine rich sequences [62]. MZ735 would instead allow a general inhibition of sequences with its non-specificity. Potential prospects for future research would be to obtain a structure with poly-pyrimidine RNA as the only structures currently are with poly-purine RNA. MZ735 or pateamine-based ligands would be ideal for this purpose because they do not have specificity. Although pateamine A-like compounds interact with either types, there is a reduced activity with

poly-pyrimidine, and with structural data, it might be possible to improve its affinity. This would potentially allow targeting of poly-pyrimidine sequences, or even specific combinations. It would also be informative if structures with the other ligands (pateamine A, DMDA-patA) were obtained confirming the structural relationship with their respective activities and would provide more information on making the ideal candidate for a potential anti-cancer development. Previously, although pateamine A was much more potent as a drug compared DMDA-patA, it is toxic to normal B and T cells [82]. DMDA-patA was less toxic to cell but binds considerably to blood plasma (99.7% to human and 99.1% to bovine), making its availability much lower [82]. Moving forward, it would be necessary to characterize MZ735 in its cellular availability (as pateamine A and DMDA-patA bind substantially to blood plasma) and as mentioned in the SAR studies, its solubility, before it undergoes further consideration in pre-clinical trials.

# 6 Conclusion

The goals of this research were to obtain a better understanding of inhibitor interaction with eIF4A. Hippuristanol was chosen for this endeavor; a potential anticancer compound with some previous structural research, and MZ735; a compound which inhibited eIF4A in a similar fashion to rocaglamide, which was recently crystallized with eIF4A. Using previously reported conditions, we were unable to confirm the presence of the hippuristanol in the structure. This might need more specialized screens/conditions to crystallize. On the other hand, we were able to crystallize the same human eIF4A construct that was previously crystallized with rocaglamide, with MZ735, a pateamine A variant, in similar (ammonium sulfate) conditions. From the obtained structure, we determined a potential site in which MZ735 interacts with eIF4A, which closely mimics the same binding site rocaglamide occupies, even though the compounds vary greatly in chemical structure. This might explain why pateamine A and rocaglamide inhibit eIF4A in a similar fashion and have mutations which render 4A cross-resistant to both compounds. There was also a potential explanation for why pateamine A does not display the same RNA selectivity that rocaglamide A possesses and possible reasons for the gain in potency when comparing to similar compounds. Potential avenues for structure-activity relationships were presented and will need further testing to determine if the suggested changes will lead to enhanced potency. Potential future research avenues would be to obtain crystal structures of other compounds like MZ735 (pateamine A in particular) to further understand the intricacies of the different substitutions. Structures with poly-pyrimidine RNA would also be very interesting to compare if any major structural changes are present and if the interactions with pateamine A are similar. This research has yielded insight on pateamine A-like ligand binding and will hopefully lead into further structural research with this category of ligands.

# 7 References


1. Grifo, J.A., et al., *New initiation factor activity required for globin mRNA translation.* J Biol Chem, 1983. **258**(9): p. 5804-10.
2. Jackson, R.J., C.U. Hellen, and T.V. Pestova, *The mechanism of eukaryotic translation initiation and principles of its regulation.* Nat Rev Mol Cell Biol, 2010. **11**(2): p. 113-27.
3. Padilla, M., et al., *Initiation factor eIF-4B (IF-M3)-dependent recognition and translation of capped versus uncapped eukaryotic mRNAs.* J Biol Chem, 1978. **253**(17): p. 5939-45.
4. Richter, N.J., et al., *Further biochemical and kinetic characterization of human eukaryotic initiation factor 4H.* J Biol Chem, 1999. **274**(50): p. 35415-24.
5. Waldron, J.A., F. Raza, and J. Le Quesne, *eIF4A alleviates the translational repression mediated by classical secondary structures more than by G-quadruplexes.* Nucleic Acids Res, 2018. **46**(6): p. 3075-3087.
6. Mader, S., et al., *The translation initiation factor eIF-4E binds to a common motif shared by the translation factor eIF-4 gamma and the translational repressors 4E-binding proteins.* Mol Cell Biol, 1995. **15**(9): p. 4990-7.
7. Tarun, S.Z., Jr. and A.B. Sachs, *Association of the yeast poly(A) tail binding protein with translation initiation factor eIF-4G.* EMBO J, 1996. **15**(24): p. 7168-77.
8. Lamphear, B.J., et al., *Mapping of functional domains in eukaryotic protein synthesis initiation factor 4G (eIF4G) with picornaviral proteases. Implications for cap-dependent and cap-independent translational initiation.* J Biol Chem, 1995. **270**(37): p. 21975-83.
9. Pelletier, J., et al., *Targeting the eIF4F translation initiation complex: a critical nexus for cancer development.* Cancer Res, 2015. **75**(2): p. 250-63.
10. Rogers, G.W., Jr., et al., *Modulation of the helicase activity of eIF4A by eIF4B, eIF4H, and eIF4F.* J Biol Chem, 2001. **276**(33): p. 30914-22.
11. Marintchev, A., et al., *Topology and regulation of the human eIF4A/4G/4H helicase complex in translation initiation.* Cell, 2009. **136**(3): p. 447-60.
12. Dmitriev, S.E., et al., *Assembly of 48S translation initiation complexes from purified components with mRNAs that have some base pairing within their 5' untranslated regions.* Mol Cell Biol, 2003. **23**(24): p. 8925-33.
13. Sun, Y., et al., *The eukaryotic initiation factor eIF4H facilitates loop-binding, repetitive RNA unwinding by the eIF4A DEAD-box helicase.* Nucleic Acids Res, 2012. **40**(13): p. 6199-207.
14. Galicia-Vazquez, G., J. Chu, and J. Pelletier, *eIF4AII is dispensable for miRNA-mediated gene silencing.* RNA, 2015. **21**(10): p. 1826-33.
15. Williams-Hill, D.M., et al., *Differential expression of the murine eukaryotic translation initiation factor isogenes eIF4A(I) and eIF4A(II) is dependent upon cellular growth status.* Arch Biochem Biophys, 1997. **338**(1): p. 111-20.
16. Chan, C.C., et al., *eIF4A3 is a novel component of the exon junction complex.* RNA, 2004. **10**(2): p. 200-9.
17. Hay, N. and N. Sonenberg, *Upstream and downstream of mTOR.* Genes Dev, 2004. **18**(16): p. 1926-45.
18. Duncan, R. and J.W. Hershey, *Identification and quantitation of levels of protein synthesis initiation factors in crude HeLa cell lysates by two-dimensional polyacrylamide gel electrophoresis.* J Biol Chem, 1983. **258**(11): p. 7228-35.
19. Haghighat, A., et al., *Repression of cap-dependent translation by 4E-binding protein 1: competition with p220 for binding to eukaryotic initiation factor-4E.* EMBO J, 1995. **14**(22): p. 5701-9.

20. Zarogoulidis, P., et al., *mTOR pathway: A current, up-to-date mini-review (Review).* Oncol Lett, 2014. **8**(6): p. 2367-2370.
21. Shahbazian, D., et al., *eIF4B controls survival and proliferation and is regulated by proto-oncogenic signaling pathways.* Cell Cycle, 2010. **9**(20): p. 4106-9.
22. van Gorp, A.G., et al., *AGC kinases regulate phosphorylation and activation of eukaryotic translation initiation factor 4B.* Oncogene, 2009. **28**(1): p. 95-106.
23. Raught, B., et al., *Phosphorylation of eucaryotic translation initiation factor 4B Ser422 is modulated by S6 kinases.* EMBO J, 2004. **23**(8): p. 1761-9.
24. Ling, J., S.J. Morley, and J.A. Traugh, *Inhibition of cap-dependent translation via phosphorylation of eIF4G by protein kinase Pak2.* EMBO J, 2005. **24**(23): p. 4094-105.
25. Karim, M.M., et al., *A mechanism of translational repression by competition of Paip2 with eIF4G for poly(A) binding protein (PABP) binding.* Proc Natl Acad Sci U S A, 2006. **103**(25): p. 9494-9.
26. Yang, H.S., et al., *The transformation suppressor Pdcd4 is a novel eukaryotic translation initiation factor 4A binding protein that inhibits translation.* Mol Cell Biol, 2003. **23**(1): p. 26-37.
27. Dorrello, N.V., et al., *S6K1- and betaTRCP-mediated degradation of PDCD4 promotes protein translation and cell growth.* Science, 2006. **314**(5798): p. 467-71.
28. Liu, P., et al., *Targeting the phosphoinositide 3-kinase pathway in cancer.* Nat Rev Drug Discov, 2009. **8**(8): p. 627-44.
29. Santarpia, L., S.M. Lippman, and A.K. El-Naggar, *Targeting the MAPK-RAS-RAF signaling pathway in cancer therapy.* Expert Opin Ther Targets, 2012. **16**(1): p. 103-19.
30. Wang, Q., et al., *Down-regulation of programmed cell death 4 leads to epithelial to mesenchymal transition and promotes metastasis in mice.* Eur J Cancer, 2013. **49**(7): p. 1761-70.
31. Yu, H., et al., *Helicobacter pylori promotes epithelial-mesenchymal transition in gastric cancer by downregulating programmed cell death protein 4 (PDCD4).* PLoS One, 2014. **9**(8): p. e105306.
32. Guri, Y. and M.N. Hall, *mTOR Signaling Confers Resistance to Targeted Cancer Drugs.* Trends Cancer, 2016. **2**(11): p. 688-697.
33. Fumarola, C., et al., *Targeting PI3K/AKT/mTOR pathway in non small cell lung cancer.* Biochem Pharmacol, 2014. **90**(3): p. 197-207.
34. Konicek, B.W., C.A. Dumstorf, and J.R. Graff, *Targeting the eIF4F translation initiation complex for cancer therapy.* Cell Cycle, 2008. **7**(16): p. 2466-71.
35. Bordeleau, M.E., et al., *Stimulation of mammalian translation initiation factor eIF4A activity by a small molecule inhibitor of eukaryotic translation.* Proc Natl Acad Sci U S A, 2005. **102**(30): p. 10460-5.
36. Bordeleau, M.E., et al., *Functional characterization of IRESes by an inhibitor of the RNA helicase eIF4A.* Nat Chem Biol, 2006. **2**(4): p. 213-20.
37. Bordeleau, M.E., et al., *Therapeutic suppression of translation initiation modulates chemosensitivity in a mouse lymphoma model.* J Clin Invest, 2008. **118**(7): p. 2651-60.
38. Tanner, N.K. and P. Linder, *DExD/H box RNA helicases: from generic motors to specific dissociation functions.* Mol Cell, 2001. **8**(2): p. 251-62.
39. Rocak, S. and P. Linder, *DEAD-box proteins: the driving forces behind RNA metabolism.* Nat Rev Mol Cell Biol, 2004. **5**(3): p. 232-41.
40. Byrd, D.R., et al., *Structure-function analysis of Escherichia coli DNA helicase I reveals non-overlapping transesterase and helicase domains.* J Biol Chem, 2002. **277**(45): p. 42645-53.
41. Theissen, B., et al., *Cooperative binding of ATP and RNA induces a closed conformation in a DEAD box RNA helicase.* Proc Natl Acad Sci U S A, 2008. **105**(2): p. 548-53.
42. Karow, A.R. and D. Klostermeier, *A conformational change in the helicase core is necessary but not sufficient for RNA unwinding by the DEAD box helicase YxiN.* Nucleic Acids Res, 2009. **37**(13): p. 4464-71.

43. Aregger, R. and D. Klostermeier, *The DEAD box helicase YxiN maintains a closed conformation during ATP hydrolysis.* Biochemistry, 2009. **48**(45): p. 10679-81.
44. Wolfe, A.L., et al., *RNA G-quadruplexes cause eIF4A-dependent oncogene translation in cancer.* Nature, 2014. **513**(7516): p. 65-70.
45. Rubio, C.A., et al., *Transcriptome-wide characterization of the eIF4A signature highlights plasticity in translation regulation.* Genome Biol, 2014. **15**(10): p. 476.
46. Cunningham, T.A., E. Chapman, and J.H. Schatz, *eIF4A inhibition: ready for primetime?* Oncotarget, 2018. **9**(85): p. 35515-35516.
47. Jiang, C., et al., *Targeting the N Terminus of eIF4AI for Inhibition of Its Catalytic Recycling.* Cell Chem Biol, 2019.
48. Cencic, R. and J. Pelletier, *Hippuristanol - A potent steroid inhibitor of eukaryotic initiation factor 4A.* Translation (Austin), 2016. **4**(1): p. e1137381.
49. Gonzalez, N., et al., *New cytotoxic steroids from the gorgonian Isis hippuris. Structure-activity studies.* Tetrahedron, 2001. **57**(16): p. 3487-3497.
50. Lindqvist, L., et al., *Selective pharmacological targeting of a DEAD box RNA helicase.* PLoS One, 2008. **3**(2): p. e1583.
51. Li, W., et al., *Structural and stereochemical requirements of the spiroketal group of hippuristanol for antiproliferative activity.* Bioorg Med Chem Lett, 2010. **20**(10): p. 3112-5.
52. Higa, T., et al., *Hippuristanols, cytotoxic polyoxygenated steroids from the gorgonian Isis hippuris.* 1981. **10**(11): p. 1647-1650.
53. Tsumuraya, T., et al., *Effects of hippuristanol, an inhibitor of eIF4A, on adult T-cell leukemia.* Biochem Pharmacol, 2011. **81**(6): p. 713-22.
54. Naineni, S.K., et al., *A comparative study of small molecules targeting eIF4A.* RNA, 2020. **26**(5): p. 541-549.
55. Robert, F., et al., *Translation initiation factor eIF4F modifies the dexamethasone response in multiple myeloma.* Proc Natl Acad Sci U S A, 2014. **111**(37): p. 13421-6.
56. Chu, J., et al., *Translation Inhibition by Rocaglates Is Independent of eIF4E Phosphorylation Status.* Mol Cancer Ther, 2016. **15**(1): p. 136-41.
57. Iwasaki, S., S.N. Floor, and N.T. Ingolia, *Rocaglates convert DEAD-box protein eIF4A into a sequence-selective translational repressor.* Nature, 2016. **534**(7608): p. 558-61.
58. Chu, J., et al., *Amidino-Rocaglates: A Potent Class of eIF4A Inhibitors.* Cell Chem Biol, 2019. **26**(11): p. 1586-1593 e3.
59. Cencic, R., et al., *Antitumor activity and mechanism of action of the cyclopenta[b]benzofuran, silvestrol.* PLoS One, 2009. **4**(4): p. e5223.
60. Saradhi, U.V., et al., *Characterization of silvestrol pharmacokinetics in mice using liquid chromatography-tandem mass spectrometry.* AAPS J, 2011. **13**(3): p. 347-56.
61. Lucas, D.M., et al., *The novel plant-derived agent silvestrol has B-cell selective activity in chronic lymphocytic leukemia and acute lymphoblastic leukemia in vitro and in vivo.* Blood, 2009. **113**(19): p. 4656-66.
62. Iwasaki, S., et al., *The Translation Inhibitor Rocaglamide Targets a Bimolecular Cavity between eIF4A and Polypurine RNA.* Mol Cell, 2019. **73**(4): p. 738-748 e9.
63. Kuznetsov, G., et al., *Potent in vitro and in vivo anticancer activities of des-methyl, des-amino pateamine A, a synthetic analogue of marine natural product pateamine A.* Mol Cancer Ther, 2009. **8**(5): p. 1250-60.
64. Low, W.K., et al., *Inhibition of eukaryotic translation initiation by the marine natural product pateamine A.* Mol Cell, 2005. **20**(5): p. 709-22.

65. Low, W.K., et al., *Second-generation derivatives of the eukaryotic translation initiation inhibitor pateamine A targeting eIF4A as potential anticancer agents.* Bioorg Med Chem, 2014. **22**(1): p. 116-25.
66. Kim, Y.R., et al., *Silencing Oncogene Translation Using Pateamine a Analogues As a Novel Therapeutic Strategy for c-Myc Driven Lymphoma.* Blood, 2017. **130**(Supplement 1): p. 4111-4111.
67. Merrick, W.C., *eIF4F: a retrospective.* J Biol Chem, 2015. **290**(40): p. 24091-9.
68. Gruner, S., et al., *The Structures of eIF4E-eIF4G Complexes Reveal an Extended Interface to Regulate Translation Initiation.* Mol Cell, 2016. **64**(3): p. 467-479.
69. Nielsen, K.H., et al., *Synergistic activation of eIF4A by eIF4B and eIF4G.* Nucleic Acids Res, 2011. **39**(7): p. 2678-89.
70. Lomakin, I.B., C.U. Hellen, and T.V. Pestova, *Physical association of eukaryotic initiation factor 4G (eIF4G) with eIF4A strongly enhances binding of eIF4G to the internal ribosomal entry site of encephalomyocarditis virus and is required for internal initiation of translation.* Mol Cell Biol, 2000. **20**(16): p. 6019-29.
71. Benz, J., H. Trachsel, and U. Baumann, *Crystal structure of the ATPase domain of translation initiation factor 4A from Saccharomyces cerevisiae--the prototype of the DEAD box protein family.* Structure, 1999. **7**(6): p. 671-9.
72. Johnson, E.R. and D.B. McKay, *Crystallographic structure of the amino terminal domain of yeast initiation factor 4A, a representative DEAD-box RNA helicase.* RNA, 1999. **5**(12): p. 1526-34.
73. Caruthers, J.M., E.R. Johnson, and D.B. McKay, *Crystal structure of yeast initiation factor 4A, a DEAD-box RNA helicase.* Proc Natl Acad Sci U S A, 2000. **97**(24): p. 13080-5.
74. Schutz, P., et al., *Crystal structure of the yeast eIF4A-eIF4G complex: an RNA-helicase controlled by protein-protein interactions.* Proc Natl Acad Sci U S A, 2008. **105**(28): p. 9564-9.
75. Oberer, M., A. Marintchev, and G. Wagner, *Structural basis for the enhancement of eIF4A helicase activity by eIF4G.* Genes Dev, 2005. **19**(18): p. 2212-23.
76. Andreou, A.Z. and D. Klostermeier, *The DEAD-box helicase eIF4A: paradigm or the odd one out?* RNA Biol, 2013. **10**(1): p. 19-32.
77. Prat, A., et al., *Expression of translation initiation factor 4A from yeast and mouse in Saccharomyces cerevisiae.* Biochim Biophys Acta, 1990. **1050**(1-3): p. 140-5.
78. Chang, J.H., et al., *Crystal structure of the eIF4A-PDCD4 complex.* Proc Natl Acad Sci U S A, 2009. **106**(9): p. 3148-53.
79. Schutz, P., et al., *Comparative structural analysis of human DEAD-box RNA helicases.* PLoS One, 2010. **5**(9).
80. Liebschner, D., et al., *Macromolecular structure determination using X-rays, neutrons and electrons: recent developments in Phenix.* Acta Crystallogr D Struct Biol, 2019. **75**(Pt 10): p. 861-877.
81. Tlais, S.F. and G.B. Dudley, *Stereocontrol of 5,5-spiroketals in the synthesis of cephalosporolide H epimers.* Org Lett, 2010. **12**(20): p. 4698-701.
82. Chen, R., et al., *Creating novel translation inhibitors to target pro-survival proteins in chronic lymphocytic leukemia.* Leukemia, 2019. **33**(7): p. 1663-1674.

# 8 Appendix

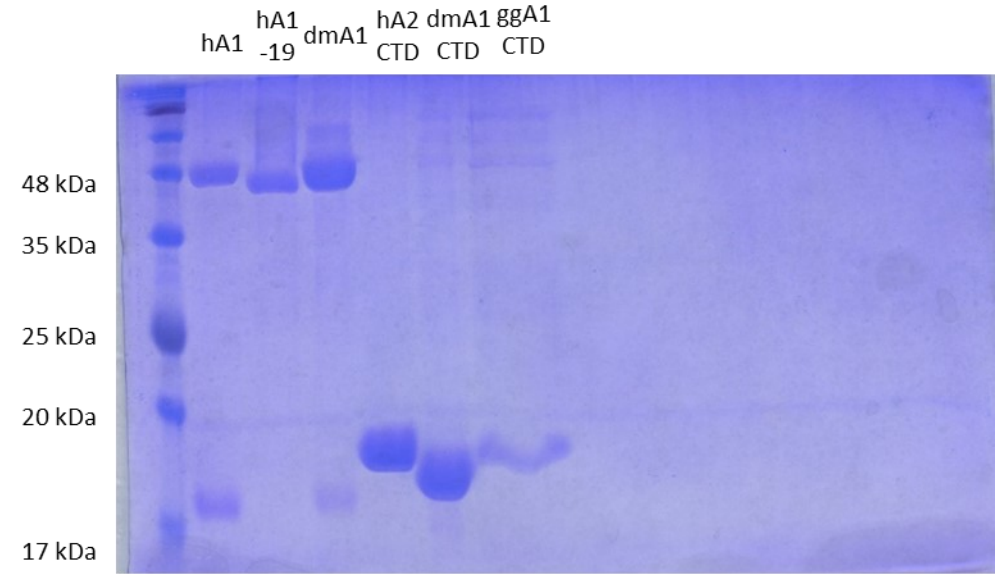


**A1. Purified eIF4A of other species**

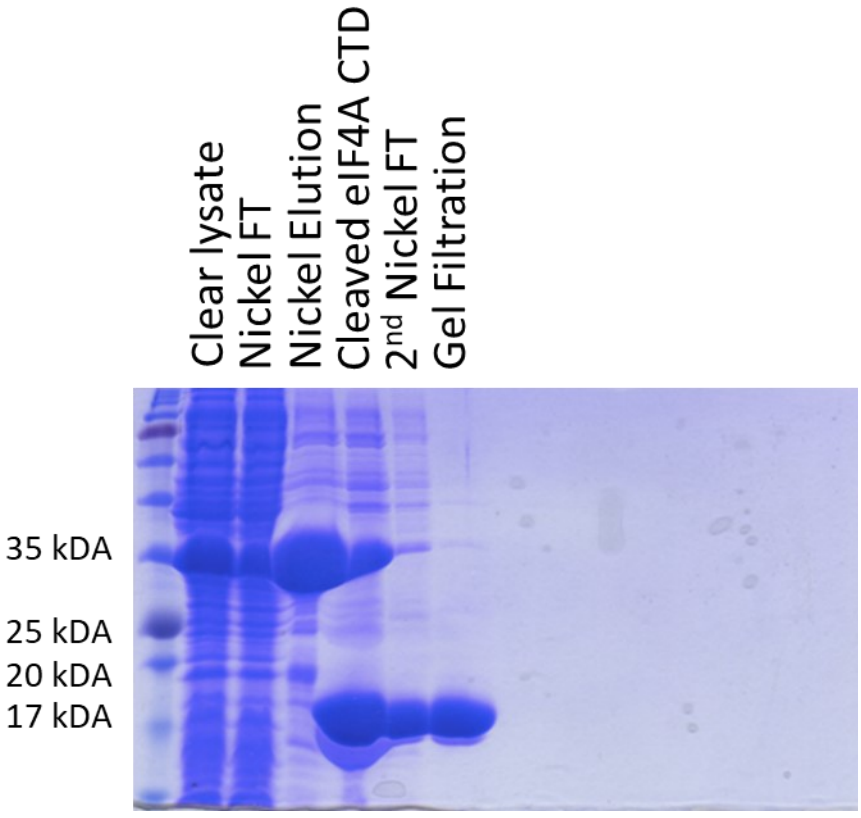


**A2. Yeast eIF4A CTD purification**

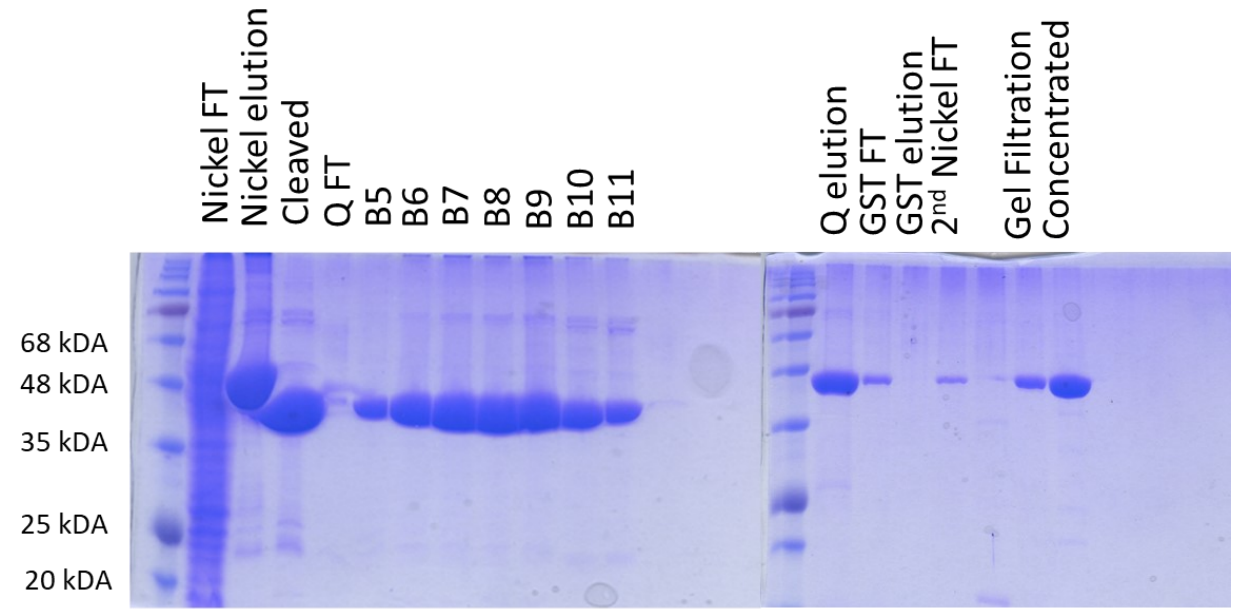


**A3. Human eIF4A Δ19 purification**

**A4. Data collection and refinement statistics**

| | Hippuristanol | MZ735 |
|---|---|---|
| **Data collection** | | |
| Space group | P1 | I222 |
| Cell dimensions | | |
| *a*, *b*, *c* (Å) | 32.517, 36.215, 62.216 | 66.8, 99.9, 153.7 |
| α, β, γ (°) | 88.328, 73.644, 89.96 | 90, 90, 90 |
| Resolution (Å) | 30.54 - 2.30 (2.38 - 2.30) | 46.5 - 2.935 (3.04 – 2.935) |
| $R_{merge}$ | 0.160 (0.233) | 0.182 (0.864) |
| $R_{meas}$ | 0.212 (0.304) | 0.190 (0.914) |
| $R_{pim}$ | 0.137 (0.195) | 0.054 (0.288) |
| CC1/2 | (0.807) | 0.984 (0.811) |
| $I / \sigma I$ | 6.45 (3.09) | 12.25 (1.4) |
| Completeness (%) | 78.0 (64.5) | 96.6 (76.6) |
| Redundancy | 1.7 (1.7) | 11.4 (7.8) |

| | | |
|---|---|---|
| **Refinement** | | |
| Resolution (Å) | 30.54 - 2.269 (2.35-2.27) | 45.58 - 2.87 (2.98 – 2.87) |
| No. reflections | 9779 (774) | 9960 (596) |
| | 973 (80) | |
| $R_{work}$ / $R_{free}$ | 0.2491 / 0.2746 (0.2756 / 0.3296) | 0.2104 / 0.2566 (0.2862 / 0.3184) |
| No. atoms | | |
| Protein | 2752 | 3244 |
| Ligand/ion | 1 | 70 |
| Solvent | 99 | 24 |
| *B*-factors | | |
| Protein | 23.89 | 60.34 |
| Ligand/ion | | 52.90 |
| Water | 23.62 | 22.35 |
| R.m.s. deviations | | |
| Bond lengths (Å) | 0.003 | 0.002 |
| Bond angles (°) | 0.76 | 0.45 |